Application of Noble Gases to the Viability of CO_2 Storage

Greg Holland and Stuart Gilfillan

Abstract

Unequivocable evidence for warming of the climate system is a reality. An important factor for reducing this warming is mitigation of anthropogenic CO_2 in the atmosphere. This requires us to engineer technologies for capture of our carbon emissions and identify reservoirs for storing these captured emissions. This chapter reviews advances made in understanding multiphase interactions and processes operating in a variety of subsurface reservoirs using noble gases. We begin by discussing the types of reservoir available for carbon storage and the mechanisms of viable CO_2 storage, before summarising the physical chemistry involved in data interpretation and the sampling/sample storage techniques and requirements critical to successful sample collection. Theory of noble gas partitioning is interspersed with examples from a variety reservoirs to aid our knowledge of long term CO_2 storage in the subsurface. These include hydrocarbon reservoir and natural CO_2 reservoirs. In these examples we show how good progress has been made in using noble gases to explain the fate of CO_2 in the subsurface, to quantify the extent of groundwater interaction and to understand CO_2 behaviour after injection into oil fields for enhanced oil recovery. We also present recent work using noble gases for monitoring of subsurface CO_2 migration and leakage in CO_2 rich soils, CO_2 rich springs and groundwaters. Noble gases are chemically inert, persistent and environmentally safe and they have the potential to be extremely useful in tracing migration of CO_2. It is imperative that the many upcoming pilot CO_2 injection studies continue to investigate the behaviour of noble gases in the subsurface and develop suitable noble gas monitoring strategies.

G. Holland (✉)
Lancaster Environment Centre, Lancaster University, Lancaster, LA1 4YQ, UK
e-mail: g.holland@lancaster.ac.uk

S. Gilfillan
School of Geosciences, University of Edinburgh, Edinburgh, EH9 3JW, UK
e-mail: stuart.gilfillan@ed.ac.uk

P. Burnard (ed.), *The Noble Gases as Geochemical Tracers*, Advances in Isotope Geochemistry,
DOI: 10.1007/978-3-642-28836-4_8,

1 Introduction

1.1 The Need for CO_2 Storage

Climate change and its effects are emerging as one of the most pressing environmental issues of the 21st century. It is generally accepted that increases in anthropogenic carbon dioxide (CO_2) emissions since the industrial revolution are a key factor in the climate warming observed to date (IPCC 2007). The period between 1995 and 2006 recorded eleven of the twelve warmest years in the instrumental record of global surface temperature, since 1850. The most recent assessment by the Intergovernmental Panel for Climate Change (IPCC) indicated that the global surface temperature has increased by 0.74 ± 0.18 °C between 1906 and 2005 (Fig. 1) (IPCC 2007). The IPCC report clearly stated "Warming of the climate system is unequivocal, as is now evident from observations of increases in global average air and ocean temperatures".

This warming of the Earth's climate has also resulted in a rise of sea levels due to melting of continental ice sheets and thermal expansion of the oceans. The 2007 IPCC report documented that global sea levels rose by 2.7 ± 0.7 mm between 1993 and 2003. The report also predicted a rise of 18–59 cm from 1990 to the 2090s, in addition to an unspecified amount that could come from partial melting of the large ice sheets covering Greenland and Antarctica. More recent studies have shown that this is probably a conservative estimate and rises of up to 1 m are not implausible (Rahmstorf 2010).

It is clear that reduction of CO_2 concentration in the atmosphere is paramount to limiting climate change in the near future and ameliorating the climate in the longer term. IPCC projections suggest a global surface temperature rise of a further 1.1–6.4 °C during the 21st century, as CO_2 concentrations rise from ~370 to ~700 ppm. This rise is largely due to global emissions of CO_2 from burning of fossil fuels at a rate of approximately 25 Gigatonnes of CO_2 equivalent per year (Marland et al. 2008). To reduce this value over the coming decades will require a combined approach of lower emissions from more fuel-efficient/alternative fuel technologies and removal of the on-going CO_2 emissions that produced as a by-product of power generation (Fig. 2).

1.2 What is Geological Carbon Storage?

Geological carbon storage is the final aspect of the Carbon Capture and Storage (CCS) process. The CCS process involves capturing CO_2 from large point source emitters such as power stations, refineries or other industrial processes,

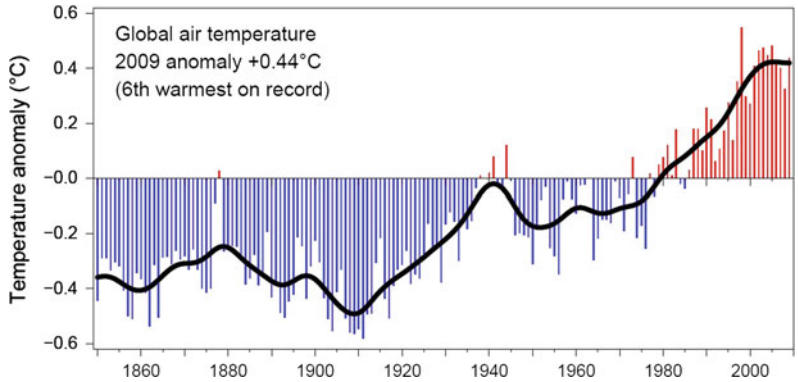

Fig. 1 This time series is compiled jointly by the Climatic Research Unit and the UK Met. Office Hadley Centre showing mean global air temperature over the last ~150 years. The record is being continually up-dated and improved (Brohan et al. 2006)

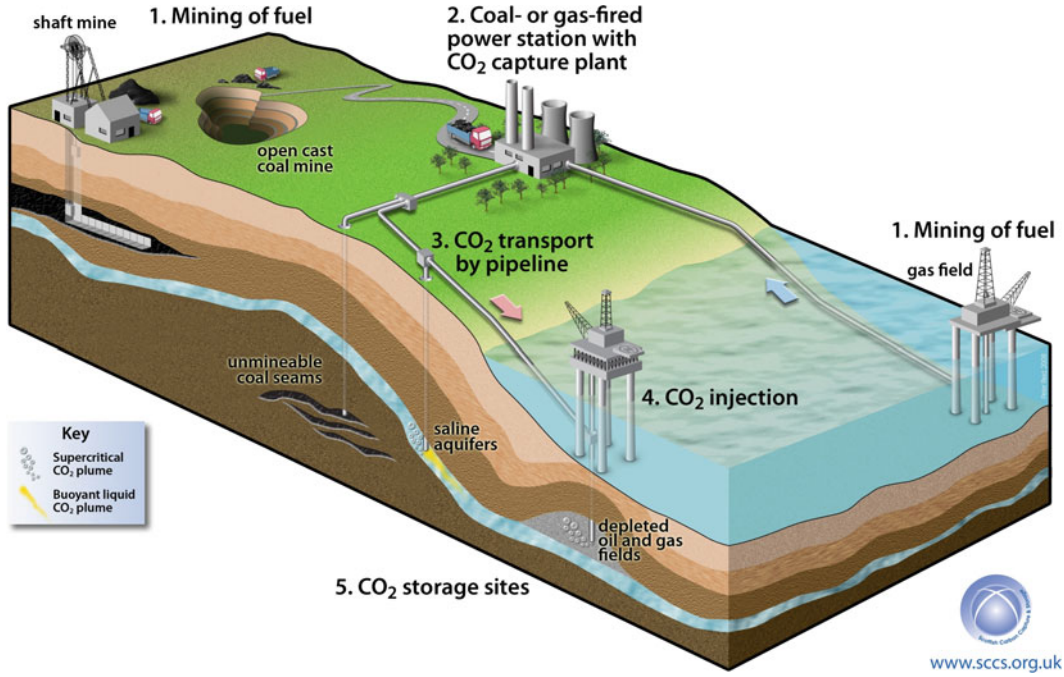

Fig. 2 Diagram illustrating the life cycle chain of fossil fuel use with carbon capture and storage technology. CO_2 capture at the point source of emission allows the CO_2 to be transported to a suitable storage reservoir. Three different subsurface storage sites are being considered and tested; (1) Empty (depleted) oil and gas reservoirs, (2) Saline aquifers and (3) Unminable coal seams. Figure credit to Scottish Carbon Capture and Storage, School of Geosciences, University of Edinburgh

compressing it to produce a supercritical fluid, then transporting, and then injecting it into geological formations that can act as natural underground storage sites. CO_2 becomes a supercritical fluid above the critical temperature of 31.1 °C and critical pressure of 7.39 MPa. Supercritical CO_2 has the properties of both a gas and a liquid, in that it expands to fill its container as a gas would whilst retaining the density of a liquid, making it easier to transport and inject than in gaseous form. The CO_2 injected into the geological carbon storage site must then remain isolated from the atmosphere for a significant period of time (1,000 to 10,000 years). In its simplest form, a geological carbon storage site will consist of a layer of permeable and porous reservoir rock situated beneath a layer of impermeable rock that will act as a seal preventing CO_2 migration to the surface.

There are three main types of proposed underground storage sites:

1.2.1 Depleted Oil and Gas Reservoirs

Oil and gas reservoirs consist of permeable and porous reservoir rocks overlain by impermeable cap rocks that have stored hydrocarbon liquids and gases over many millions of years. Those that have reached the end of their productive life are ideal for CO_2 storage. CO_2 can be pumped into the reservoirs, using the boreholes originally drilled to extract the oil and gas, to fill the empty pore space left by removal of hydrocarbons. The geology of these reservoirs is often well characterized to maximise oil recovery therefore fluid behaviour in these systems is well understood.

However, those reservoirs which have been subjected to the injection of water or gas to increase reservoir pressure and aid oil recovery may require extra production of the hydrocarbons in order to make space for the CO_2 (Haszeldine 2009). This technique is known as enhanced oil recovery (EOR) and can produce 10–15 % more oil. EOR is a mature technology

that has been operating since the early 1970s . In addition, the natural gas industry has been reliant on underground natural gas reservoirs for many decades and enhanced gas recovery (EGR) is also a viable technique. These reservoirs could also be adapted for CO_2 injection and long-term storage. Depleted oil and gas reservoirs are expected to provide potential for storing 920 Gt CO_2 (IEA 2009)—45 % of the total CO_2 output from 2000 to 2050 assuming the IEA's business as usual scenario for CO_2 emissions (i.e. no significant reduction in emissions).

1.2.2 Deep Saline Formations

Saline formations, also known as saline aquifers, are rock formations saturated with salt water that are unsuitable for supplying potable water. These exist worldwide, not just in hydrocarbon provinces and potentially could store large volumes of CO_2. CO_2 injected into these saline formations would partially dissolve into the saline water, storing the CO_2. Additionally, in some cases carbonate minerals could precipitate, locking up the CO_2 permanently. Recent estimates suggest the capacity for storage in geological reservoirs in North West Europe alone could be as much as 800 Gt CO_2 (with most of this in deep saline reservoirs), with other estimates suggesting that up to 10, 000 Gt CO_2 could be stored globally (IEA 2009). However, these estimates are probably somewhat optimistic as they assume static injection efficiency of 5–10 %, when dynamic injection of CO_2 at the Utsira aquifer in the North Sea currently fills only 0.2 % of the pore space. Further study and the injection of CO_2 into other aquifers is required to fully determine the storage capacity and long term storage viability of saline aquifers.

1.2.3 Deep (Un-Minable) Coal Seams

Injection of CO_2 into deep un-mineable coal seams is also a possibility, where the CO_2 will be stored on the surface pores and fractures of the coal. This has the additional benefit of forcing the methane, which is already present within the coal beds, from the coal and so increasing recovery of the coal bed methane. This could offset the cost of CO_2 injection and even if the additional methane extracted is not of economic use, coal can adsorb twice as much CO_2 by volume as methane. Hence, conventional coal bed methane extraction and subsequent CO_2 injection will still result in net storage of CO_2.

1.2.4 Additional CO_2 Storage Options

There are several alternative options for CO_2 storage which include biological sequestration (Marland and Schlamadinger 1999), deep ocean sequestration (Brewer et al. 1999) and CO_2 injection into deep ocean carbonate sediments (House et al. 2006) or basalts (Goldberg et al. 2008) to form carbonate minerals. However, all of these are, with the exception of ocean sequestration, in their infancy and do not offer the necessary volume or security of storage required for large scale CO_2 storage at present (Baines and Worden 2004a).

Injection of large amounts of CO_2 into the marine environment may acidify large amounts of sea water (Haszeldine 2009) and ocean storage is not a permanent method of CO_2 storage. There is a potential risk that CO_2 will over time return to atmosphere, as there is not a distinct physical barrier to prevent the CO_2 from doing so. For these reasons this method of storage has been deemed unsuitable at the current time and is currently outlawed by international marine treaties.

In this chapter we focus on the depleted oil and gas reservoirs as this is the CO_2 storage setting that has received most attention from the scientific community to date and provides important lessons directly relevant to storage in other settings.

1.3 Mechanisms of Viable CO_2 Storage

The key requirement for successful geological CO_2 storage within the Earth is the safety and security of CO_2 retention over significant timescales. It is essential that protocols for monitoring and risk assessing CO_2 storage sites and potential leakage pathways are developed. The

existence of CO_2 reservoirs that have been isolated from the atmosphere for millions of years (Ballentine et al. 2001; Gilfillan et al. 2008) demonstrates the feasibility of storing CO_2 for significant periods of time but understanding the exact behaviour of CO_2 in these systems is of paramount importance. Secure CO_2 storage can be achieved by ensuring that the stored CO_2 is immobile and trapped by one of the four mechanisms outlined below.

1.3.1 Physical Trapping: Stratigraphic and Structural Storage

Supercritical CO_2 has a lower density than water, so when CO_2 is injected into a reservoir it will ascend through the microscopic pore spaces between the grains in the reservoir rock to the top of the reservoir. Therefore, it is essential that a suitable impermeable cap rock such as a shale, clay or mudstone overlies the reservoir to act as a physical barrier to the CO_2 and prevent migration of the CO_2 from the reservoir. Cap rocks of oil and gas fields have trapped buoyant hydrocarbon fluids in this manner for millions of years.

1.3.2 Residual or Hydrodynamic Storage

Microscopic pore spaces which exist between grains in the reservoir rock are analogous to a foam sponge. CO_2 can enter 'dead end' pores in a similar fashion to how air is trapped within a foam sponge. This is known as residual trapping and is the reason why soaking a sponge in water cannot be achieved by submersing it: the sponge requires squeezing to expel the residually trapped air and replace it with water.

1.3.3 Dissolution Storage or Solubility Trapping

As CO_2 is readily soluble in water, it will dissolve in the formation water trapped in the pore spaces within a reservoir. The water containing dissolved CO_2 is denser than the formation water surrounding it. This dense water sinks to the bottom of the reservoir, trapping the CO_2. Provided that the formation water does not migrate from the reservoir this is a secure trapping mechanism.

1.3.4 Mineral Storage or Mineral Trapping

CO_2 dissolves in water to form a weak acid (carbonic acid) and this acid can dissolve and react with the mineral grains present in the reservoir rock. The reaction of the bicarbonate ions produced when the CO_2 dissolves into the formation water with calcium, magnesium and iron from silicate minerals such as micas, clays, feldspars and chlorites will form carbonate minerals. These will be produced in the interior of pores in the reservoir rock and have the potential to 'lock away' the CO_2 within the rock. This is the most permanent trapping mechanism. However, under normal reservoir conditions this process is very slow, typically taking thousands of years (IPCC 2005).

2 Sample Collection and Analytical Techniques

Within the Colorado Plateau and surrounding Rocky Mountain region there are at least nine producing or abandoned gas fields that contain up to 2,800 billion m^3 of natural CO_2 (Allis et al. 2001). These fields act as a natural analogues of CO_2 repository sites and hence intensive studies have been undertaken to provide an understanding of CO_2 behaviour within them. Data included in this chapter are predominantly from five producing gas fields, namely McCallum Dome, (Jackson Co, CO); Sheep Mountain, (Huerfano County, CO); Bravo Dome, (Harding County, NM); McElmo Dome and the related field Doe Canyon, (Montezuma County, CO); St Johns Dome (Apache County, AZ) and eight natural CO_2 seeps at Green River, (Emery and Grand Counties, UT). All of these sites produce CO_2 in extremely high concentrations, averaging 95–99 % CO_2, 1–4 % N_2, 0.1–1 % He and other trace gases (Allis et al. 2001). The majority of these samples were taken directly from producing wellheads that tap the natural gas reservoirs, although samples from several 'shut in' wellheads with high gas pressures were also collected. Well sample sites were chosen on site to

provide a wide range of depths and spatial distribution across the individual reservoirs. Two field-sampling techniques were used to collect these samples.

2.1 Well Head Collection Methods

The first method utilized 'Swagelok©' 300 ml stainless steel sampling cylinders sealed at both ends with high-pressure valves. The cylinders were baked at 150 °C and evacuated prior to sampling use. The cylinders were attached directly to the wellheads before the gas had undergone any form of processing. A length of high pressure hosing was attached to the other end of the cylinder to act as an exhaust. The cylinders were then flushed with gas from the wellhead for 5 min and then purged 6 times. The purging process involves filling the cylinder with well gas, closing the valve to the wellhead, and then releasing the gas. This ensured that there is virtually no air contamination present in the sample. This method was used for wellheads that have high flow rates and typical wellhead pressures ranged from 1.38 to 3.45 MPa.

2.2 Water and Low Pressure Gas Collection Methods

The second collection technique used a 70 cm long piece of 3/8″ diameter refrigeration grade copper tubing as the sample container. This method was used for sampling of low-pressure wellheads with lower flow rates and the Green River seeps. The copper tubing is contained in an aluminium holder with clamping devices at each end and provides approximately 10 cm^3 of gas for analysis (Fig. 3). In the field, high pressure hosing was secured to one end of the copper tubing, which was connected to a gas regulator attached directly to the wellhead by a suitable adapter. The remaining end of the tubing was connected to another section of tubing with a second length of high pressure hosing so a duplicate sample could be obtained. A third length of high pressure hosing was attached to the second length of copper tubing to act as an exhaust and prevent turbulent backflow of atmospheric gases into the sample. Gas from the wellhead was then pumped into both sections of tubing at a regulated pressure of 0.20 MPa (2 atm). The entire line was flushed with gas from the wellhead for 10 min. After flushing, the clamp furthest from the wellhead was closed sealing the end of the copper tube by cold welding. The other clamps were then shut in turn working back up the line to the wellhead. These clamps are then left closed until the samples are ready for analysis. Secure sample storage is achieved as copper is virtually impervious to noble gases (Hilton et al. 2002). Sample analysis was carried out by connecting one end of the copper tube to the mass spectrometer and releasing one of the clamps.

The Green River seeps (Sect. 7.1) were collected using a similar copper tube procedure. All of the seeps were actively releasing CO_2 within pools of water. To sample this gas a plastic funnel connected to a length of high pressure hosing was positioned over the bubbling gas, and submerged into the water. The water provides a seal from the atmosphere, preventing air contamination of the samples. The high pressure hose was directly connected to two copper tubes, allowing duplicate samples to be collected. Gas was allowed to flow freely into the copper tubes for a minimum of 10 min. The clamps were then shut sequentially working back from the clamp furthest from the seep. The water samples collected at St. Johns Dome (Sect. 7.3) and on the Kerr property (Sect. 7.4) were collected in the same manner using copper tubes after flowing water through the tubes for 5 min. The samples were either taken directly from producing well heads or from depth in groundwater pools or wells using a peristaltic pump and a weighed piece of hosing.

2.3 Issues of Long Term Sample Storage

Collection using the high pressure cylinder technique has been the convention in both the commercial and academic sectors. However, re-analysis of a suite of well gas samples after several years of lab storage has highlighted a serious issue, specifically that the double valved

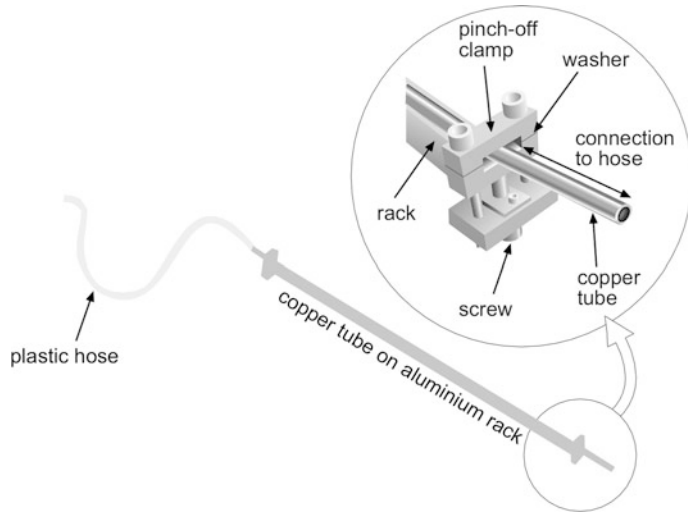

Fig. 3 Schematic of the apparatus used for noble gas sampling with copper tubing [from Becker (2005)]. The plastic hose is attached directly to the well head using a suitable regulator, CO_2 gas is allowed to flow through the copper tube until sample collection is complete. The tubing is then crimped at both ends

Swagelok cylinder approach is prone to air contamination. Over a period of two years, between summer 2005 and summer 2007, samples with $^{40}Ar/^{36}Ar$ ratio of ~22, 000 had been reduced by ingress of air to a $^{40}Ar/^{36}Ar$ ratio ~3,000. The mechanism by which this air contamination had occurred was not specifically identified, but because the partial pressure of noble gases in the atmosphere is significantly higher than in the well gases, any pathway for noble gas transfer will result in an influx of atmospheric noble gases to the cylinders. The high pressure valves were attached to the cylinders via steel screw threads wrapped in PTFE tape and the valve tips were also Teflon based. In a noble gas world where all metal systems are the norm, including linkages and valve tips, it is likely that one or both of these potential weak points are the source of the contamination. Samples are still collected in high pressure cylinders as required by health and safety issues at point of collection and due to commercial shipping regulations but in an attempt to alleviate this problem, the gases are rapidly transferred to an all metal storage device (currently metal spheres with a welded Conflat fitting and a standard copper tipped valve).

2.4 Analytical Techniques Specific to CO_2 Samples

At the University of Manchester, where some of the work reported in this chapter was undertaken, a specific vacuum line was constructed to handle the clean-up requirements of large volumes of well gas. This consisted of a calibrated volume containing a high pressure Baratron® capacitance manometer, a Ti sponge furnace, a Zr-Al SAES getter, cold finger, a quadrupole mass spectrometer and both an ion and turbo pump. The quadrupole was essential for ensuring that the samples had been cleaned up thoroughly prior to admission into the mass spectrometer clean-up/gas extraction line. The separate pumping system also ensured that no hydrocarbon or CO_2 was able to enter the main clean up line.

Well gas samples were extracted from either the copper sample tubes or from stainless steel cylinders into the volume containing a high

pressure Baratron® capacitance manometer. The pressure was recorded, allowing calculation of the volume of CO_2 administered. The sample was then expanded onto a Ti sponge furnace to remove CO_2 and any other active gases. This furnace was preheated to 1,173 K (900 °C) with each sample held at this temperature for 10 min, and then cooled to room temperature over a period of 15 min. Approximately 10 g of Ti sponge material was capable of removing 1 L of CO_2, permitting multiple analyses of the same sample and high precision analyses of the rarer noble gas isotopes of Kr and Xe. These volumes of CO_2 would quickly saturate a Zr-Al SAES getter typically found on noble gas extraction lines and is a necessary step in preparation of CO_2 well gas samples for analysis. Subsequently, the sample was exposed for 10 min with a Zr-Al SAES getter heated to 523 K.

3 Noble gases in Geological Reservoirs

3.1 Introduction

Noble gases are chemically inert elements that exist as extremely volatile gases at standard temperature and pressure. Their lack of reactivity results in no change in their isotopic compositions via chemical processes but allows them to be used as a tracer of physical processes, which can alter both their isotopic and relative elemental compositions. In the context of storage in geological reservoirs, their relative abundances are sensitive to partitioning between different fluid phases such as oil, water and gas, enabling their use as tracers of physical processes even if they have subsequently been partitioned from their host fluids. The three key sources of noble gases in natural gas reservoir fluids are the crust, the atmosphere and the mantle. Each of these possesses different isotopic compositions permitting resolution of the different sources (see Fig. 4).

3.2 Sources of Noble Gases in a Subsurface Reservoir

Noble gases on the Earth are derived from two principle sources: those trapped during the planetary accretion process which are commonly known as ‘primitive’, ‘juvenile’ or ‘primordial’ noble gases (e.g. ^{3}He) and radiogenic noble gases generated by radioactive decay processes within the Earth (e.g. ^{4}He). The radiogenic noble gases are primarily produced by radioactive decay and nucleogenic reactions (Table 1). Minor amounts are also produced by cosmic ray spallation, although this is not relevant to study of CO_2 storage and is not discussed further. The following summary documents these main production mechanisms and focuses on the reactions that are directly relevant to the use of noble gases as tracers in natural gas and CO_2 reservoirs.

3.3 Noble Gas Production

3.3.1 Radiogenic Helium: ^{4}He

^{4}He is produced by any α—decay radioactive pathway which emits α particles. The three most significant radioactive parent isotopes are ^{238}U, ^{235}U and ^{232}Th. Both U and Th are incompatible elements which are concentrated in the continental crust. The majority of crustal rocks contain U and Th in an almost constant weight ratio of 3.3, meaning that ^{4}He production from all three nuclides can be referenced to the abundance of U alone. The ^{4}He production rate expressed in this way is 2.15×10^{-7} cm^3 per gram of U per year (Ozima and Podosek 2001).

3.3.2 Radiogenic Argon: ^{40}Ar

Radiogenic decay of another incompatible element, ^{40}K, results in the production of ^{40}Ar. ^{40}K is strongly partitioned into the crust and therefore ^{40}Ar production is highly significant despite the low isotopic abundance (0.00012) of ^{40}K and only 11 % decaying to ^{40}Ar by electron capture (with the remainder decaying by β decay to ^{40}Ca). Over geologic time the average ^{40}Ar production rate is 3.89×10^{-12} cm^3 per gram of

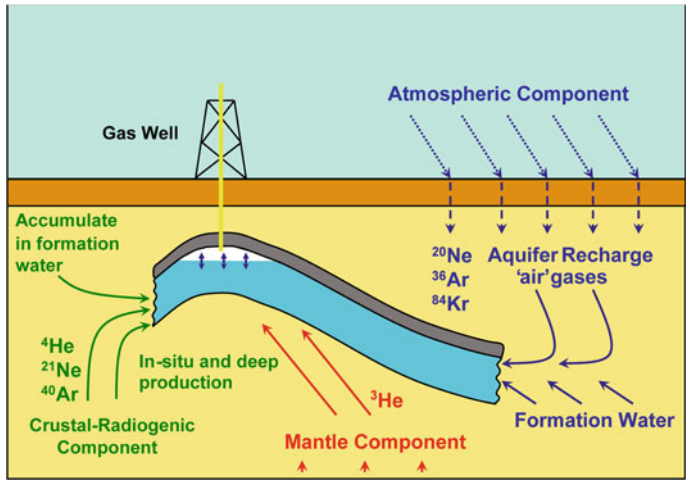

Fig. 4 Schematic diagram of a natural gas reservoir, highlighting the three distinct components and their corresponding isotopes which may occur in a natural gas reservoir. The radiogenic noble gases (e.g. ^{4}He, ^{21}Ne and ^{40}Ar) are produced within the Earth's crust by the radioactive decay of U, Th and K. Atmospheric noble gases (e.g. ^{20}Ne and ^{36}Ar) are input into the gas phase as a result of equilibration with the groundwater at recharge. Within areas of continental extension or magmatic activity mantle derived noble gases (e.g. ^{3}He) may also be present. The distinct elemental and isotopic composition of the noble gases from these three components permits the contribution from each to be quantitatively resolved from any crustal fluid (redrawn from Ballentine et al. 2002)

Table 1 Radiogenic nuclides and their half-lives for noble gases, from Porcelli et al. (2002) and references therein

Nuclide	Half-life	Daughter	Yield	Comments
^{3}H	12.26 a	^{3}He	1	Continuously produced in atmosphere
^{238}U	4.468 Ga	^{4}He	8	
		^{136}Xe	3.6×10^{-8}	Spontaneous fission
^{235}U	0.704 Ga	^{4}He	7	$^{238}U/^{235}U = 137.88$
^{232}Th	14.01 Ga	^{4}He	6	Th/U = 3.8 in bulk Earth
		^{136}Xe	$<4.2 \times 10^{-11}$	No significant production in Earth
^{40}K	1.251 Ga	^{40}Ar	0.1048	^{40}K = 0.01167 % total K
^{244}Pu	80 Ma	^{136}Xe	7.0×10^{-5}	$^{244}Pu/^{238}U = 6.8 \times 10^{-3}$ at 4.56 Ga
^{235}U	0.704 Ga	^{4}He	1	$^{129}I/^{127}I = 1.1 \times 10^{-4}$ at 4.56 Ga

K per year and this has resulted in ^{40}Ar dominating the Ar isotope budget with an isotopic abundance of 99.6 % in the atmosphere.

3.3.3 Krypton and Xenon

Small amounts of fissionogenic Xe and Kr are produced by the fission of ^{244}Pu and ^{238}U. The most significant product of these reactions is ^{136}Xe which is produced at a rate of 4.98×10^{-16} cm^{3}g^{-1}(U) a^{-1} and is accompanied by lesser amounts of ^{131}Xe, ^{132}Xe and ^{134}Xe. Minor amounts of Kr isotopes are also produced by U fission but are not relevant for these discussions so have been omitted.

3.3.4 Nucleogenic Helium and Neon

Alpha particles and neutrons emitted during the decay series of U and Th can bombard lighter elements and cause nuclear reactions producing noble gases. The production of Ne isotopes in the crust is almost entirely due to nucleogenic routes (Table 2). Their rate of production is directly related to radioelement and target-element concentrations and the distribution of the

Table 2 Nucleogenic reactions applicable to this study

Parent	Occurrence	Reaction	Noble gas
Li	Incompatible element, high concentrations in granitic rocks	$^{6}Li(n,\alpha)^{3}He$	^{3}He
O	Major constituent of all Silicates	$^{17}O(\alpha,n)^{20}Ne$	^{20}Ne
O		$^{18}O(\alpha, n)^{21}Ne$	^{21}Ne
Mg	Constituent of Ferro-magnesium rocks e.g. basalts	$^{24}Mg(n, \alpha)^{21}Ne$	^{22}Ne
Mg		$^{25}Mg(n, \alpha)^{22}Ne$	^{22}Ne
F	Igneous terranes, phosphatic and fluorite ore deposits	$^{19}F(\alpha,n)^{22}Na(\beta)^{22}Ne$	^{22}Ne

Data compilation by Ballentine and Burnard (2002) and references therein

target element related to radioelement heterogeneity (Ballentine and Burnard 2002). Additionally, in regions with high U and Th or with unusual compositions, such as high Li contents, nucleogenic ^{3}He production can increase the $^{3}He/^{4}He$ ratios.

3.4 Atmospheric Noble Gases

With the exception of He, which is lost to space, the Earth's noble gases are concentrated in the atmosphere. This is a result of their highly volatile nature, meaning that the atmosphere consists of primordial noble gases that have been outgassed from the Earth's mantle early in its history (e.g. Porcelli and Ballentine 2002) and possibly from external volatile sources such as comets (e.g. Holland et al. 2009).

The noble gas composition of the atmosphere is well constrained (Porcelli et al. 2002; Sarda et al. 1985) and is the standard used as a reference for discussion. With the exception of Ar which is dominated by radiogenic ^{40}Ar and accounts for almost 1 % of the atmosphere, the noble gases are present as trace constituents. The atmosphere contains almost the entire inventory of ^{36}Ar. The $^{40}Ar/^{36}Ar$ ratio of the atmosphere was originally equal to the solar ratio ($<10^{-3}$) but this has been increased to its present value of 295.5 by radiogenic production of ^{40}Ar (Sarda et al. 1985). The atmospheric $^{3}He/^{4}He$ value is commonly referred to as R_A (where R_A is the $^{3}He/^{4}He$ ratio of air at 1.4×10^{-6}). The He inventory of the atmosphere is a combination of material outgassed from the mantle (which is rich in ^{3}He), material produced in and outgassed from the crust (which is rich in ^{4}He), cosmogenic material (rich in ^{3}He) and material lost to space (^{3}He is preferentially lost over ^{4}He as it is lighter and more volatile). The other significant atmospheric noble gases are ^{20}Ne, ^{84}Kr, ^{129}Xe and ^{132}Xe which have characteristic ratios relative to Ar of $^{20}Ne/^{36}Ar = 0.5185$, $^{84}Kr/^{36}Ar = 0.0207$ and $^{130}Xe/^{36}Ar = 0.7237 \times 10^{-3}$ (Ozima and Podosek 2001).

Noble gases from the atmosphere are dissolved in water with the proportions dependent on their respective solubilities and subsequently migrate into basin aquifers, transported by groundwater (Mazor 1972). The fractionation of atmospheric noble gases present in the subsurface natural gases then provides information on the interaction between oil phases, if any, present in the fluid system (Ballentine et al. 1996; Pinti and Marty 1995) and the interactions between water and gas phases, as well as the extent of degassing of the groundwater.

3.5 Crustal Noble Gases

The noble gas inventory of the crust is extremely variable as it is dependent on age, geological history (e.g. degree of metamorphism) and composition of radioactive elements. U, Th and K are enriched in the crust as a result of their incompatible behaviour, and therefore so are ^{4}He and ^{40}Ar, the products of their radioactive decay. Crustal $^{3}He/^{4}He$ ratios are typically within the range of 0.01–0.05 Ra (Ozima and Podosek 2001), but can be significantly higher in Li-rich regions, due to nucleogenic production of ^{3}He (Tolstikhin et al. 1996). The present day $^{4}He/^{40}Ar$ production ratio of the lower, middle and upper crust can be calculated as 3.09, 5.79 and 6.00 (Ballentine and Burnard 2002), using the average crustal composition values of the three separate crust portions. This gives a

production weighted average value of 5.7. ^{36}Ar production in the crust is a minor component compared to the amount of atmosphere-derived ^{36}Ar that is introduced dissolved in the groundwater (Fontes et al. 1991). Fissionogenic Kr and Xe can be significant in regions rich in U, with fissionogenic Xe being characterised by a $^{136}Xe/^{132}Xe$ ratio of 1.733 ± 0.003 and $^{134}Xe/^{132}Xe$ of 1.435 ± 0.003 (Drescher et al. 1998).

3.6 Mantle Noble Gases

The presence of excess ^{129}Xe in the mantle, which is produced by the decay of the extinct ^{129}I with a half-life of 15.7 Ma, implies that the mantle outgassed very early in Earth history (<100 Ma). I–Pu–U systematics requires significant loss of noble gases over this period (Porcelli et al. 2001). Loss of almost all of the primordial ^{36}Ar to the atmosphere and radiogenic production of ^{40}Ar from the decay of ^{40}K has resulted in a high upper mantle $^{40}Ar/^{36}Ar$ ratio, with a upper limit of >35,000 (Burnard et al. 1997; Holland and Ballentine 2006; Moreira et al. 1998). The $^{3}He/^{4}He$ ratios of the mantle are also high and exhibit a distinct difference between the upper and primitive lower mantle sources. The $^{3}He/^{4}He$ signature of oceanic island basalts (OIBs) sourcing the primitive lower mantle is highly variable, typically ranging between 9–32 R_A (Farley and Craig 1994; Trieloff et al. 2000). This is in contrast to the narrow range of $\sim 8 \pm 1$ R_A exhibited by mid ocean ridge basalts (MORB) (Graham 2002), which sample the upper portion of the convective mantle.

4 Understanding the Sources and Processing of Crustal Fluids

4.1 Introduction

As described in the previous section, noble gases are predominantly derived from the atmosphere, the crust and the mantle. We have also seen that the isotopic signatures of these three reservoirs are distinct from one another. These characteristic differences in isotopic composition allow us to distinguish between components.

4.2 Two Component Mixing

The atmosphere has relatively low concentrations of radiogenic/nucleogenic noble gases ^{21}Ne, ^{40}Ar and ^{136}Xe compared to crustal sources. To distinguish between the two, the isotopic ratios can be compared with the atmospheric ratio to identify crustal excess (Ballentine et al. 2002).

In a two component crust/air mixture:

$$\left[{}^{21}Ne\right]_{crust} = \left[{}^{21}Ne\right]_{tot} \times \left[1 - \left({}^{21}Ne/{}^{20}Ne\right)_{air} / \left({}^{21}Ne/{}^{20}Ne\right)_{s}\right] \quad (1)$$

$$\left[{}^{40}Ar\right]_{crust} = \left[{}^{40}Ar\right]_{tot} \times \left[1 - \left({}^{40}Ar/{}^{36}Ar\right)_{air} / \left({}^{40}Ar/{}^{36}Ar\right)_{s}\right] \quad (2)$$

$$\left[{}^{136}Xe\right]_{crust} = \left[{}^{136}Xe\right]_{tot} \times \left[1 - \left({}^{136}Xe/{}^{130}Xe\right)_{air} / \left({}^{136}Xe/{}^{130}Xe\right)_{s}\right] \quad (3)$$

Where subscripts crust and total refer to concentrations and subscripts air and s refer to the isotopic compositions of the atmosphere and sample, respectively.

^{4}He is also produced in significant quantities in the crust but the He system is complicated by the presence of 'primitive' ^{3}He, sourced from the mantle. In order to resolve the mantle/crustal components, ^{3}He can be used. Although He has a low abundance in the atmosphere due to thermal loss, excess air corrections must still be made by using the observed air-derived ^{20}Ne concentrations (Ballentine et al. 2002).

$$\left(\frac{{}^{3}He}{{}^{4}He}\right)_{c} = \frac{\left(\left(\frac{{}^{3}He}{{}^{4}He}\right)_{s} \times \left(\frac{{}^{4}He}{{}^{20}Ne}\right)_{s}\right) \div \left(\left(\frac{{}^{4}He}{{}^{20}Ne}\right)_{air} \times \left(\frac{{}^{3}He}{{}^{4}He}\right)_{air}\right)}{\left(\left(\frac{{}^{4}He}{{}^{20}Ne}\right)_{s} - \left(\frac{{}^{4}He}{{}^{20}Ne}\right)_{air}\right) - 1} \quad (4)$$

Subscripts c, s and air refer to the corrected, measured and air-derived ratios, respectively. Once corrected for excess air, the $^{3}He/^{4}He$ ratio represents the sum of the crust and the mantle, with crustal ^{4}He given by:

$$\left[{}^{4}He\right]_{c} = \frac{\left[{}^{4}He\right]_{tot} \times \left(\left(\frac{{}^{3}He}{{}^{4}He}\right)_{mantle} - \left(\frac{{}^{3}He}{{}^{4}He}\right)_{c}\right)}{\left(\left(\frac{{}^{3}He}{{}^{4}He}\right)_{mantle} - \left(\frac{{}^{3}He}{{}^{4}He}\right)_{crust}\right)} \quad (5)$$

Where subscripts mantle, crust and c refer to the mantle, crust and air corrected values.

4.3 Three Component Mixing

In many crustal fluid reservoirs, a significant magmatic component is present in the fluids, in addition to the air and radiogenic components. Typically, all three components, including that of the atmosphere can be observed in the noble gases. In principle, it is possible to correct out the air component using an unambiguously air derived isotope. In practice, this is problematic because this correction depends on no (or at least well quantified) elemental fractionation in an individual sample which is often not the case. However, due to the large differences in isotopic composition of the mantle, crust and atmosphere end-members of Ne, this isotopic system alone can be used to make the correction for the atmospheric component (Fig. 5). This is because any sample that contains a mix of these components must plot within the envelope defined by the well-known $^{20}Ne/^{22}Ne$ and $^{21}Ne/^{22}Ne$ air and crust end members and the resolved mantle end member values of 12.5 for $^{20}Ne/^{22}Ne$ and 0.06 for $^{21}Ne/^{22}Ne$ (Ballentine et al. 2005). Hence, the Ne isotope system is a particularly useful tracer within natural gas reservoirs as the contribution from the mantle, crust and atmosphere to any sample can be resolved. In the following sections we shall see that Ne isotopic composition provides the most striking evidence of the different proportions of atmosphere, crust and mantle inputs to subsurface gas systems.

4.4 Role of Stable Isotopes

In many natural reservoirs, the dominant CO_2 source and basin scale processes that act on it are poorly constrained. This is primarily a reflection of the multiple origins of CO_2 in the subsurface which include methanogenesis, oil field biodegradation, kerogen decarboxylation, hydrocarbon oxidation, decarbonation of marine carbonates and degassing of magmatic bodies (Jenden et al. 1993; Wycherley et al. 1999). Carbon isotopes can be measured within natural CO_2 gas and precision is usually better than 0.1 ‰ (Javoy et al. 1986), the $\delta^{13}C(CO_2)$ signature having been used previously to distinguish between different CO_2 sources. However, $\delta^{13}CO_2$ values alone do not provide an unambiguous means to distinguish between mantle-derived CO_2 and CO_2 derived from crustal sources such as the metamorphism of carbonate rocks. This is due to the average mantle carbon and bulk crustal carbon exhibiting an overlapping range of $\delta^{13}CO_2$ of −3 to −8 ‰ (Fig. 6) (Sherwood Lollar et al. 1997). These are the only sources that can produce gas fields containing greater than 99 % CO_2 by volume, which are particularly pertinent as natural CO_2 sequestration analogues.

A much more unambiguous measure of CO_2 origin is provided by comparing the absolute amount of the magmatic noble gas, ^{3}He, to the CO_2 concentration within the gas reservoir, because the mantle $CO_2/^{3}He$ ratio measured in mid-ocean ridge basalts (MORB) has a small range, from 1.0×10^{9} to 1.0×10^{10} (Burnard et al. 2002; Marty and Jambon 1987; Trull et al. 1993), compared with the range observed in natural gases. Figure 7 shows $CO_2/^{3}He$ plotted against CO_2 concentration. Any natural CO_2 sample that plots above this MORB range irrespective of CO_2 content can only be attributed to a CO_2 source containing minimal ^{3}He, providing an unambiguous identification of a crustal CO_2 source. Samples within or below the MORB range contain a magmatic component but have been subjected to possible CO_2 loss, dilution (by addition of other gas species such as CH_4 or N_2) and/or crustal CO_2 addition. Careful study of both the $\delta^{13}C$ (CO_2) isotopes and $CO_2/^{3}He$ ratios can distinguish between these processes and allow CO_2 origins to be determined (Ballentine et al. 2001, 2002; Sherwood Lollar et al. 1994, 1997).

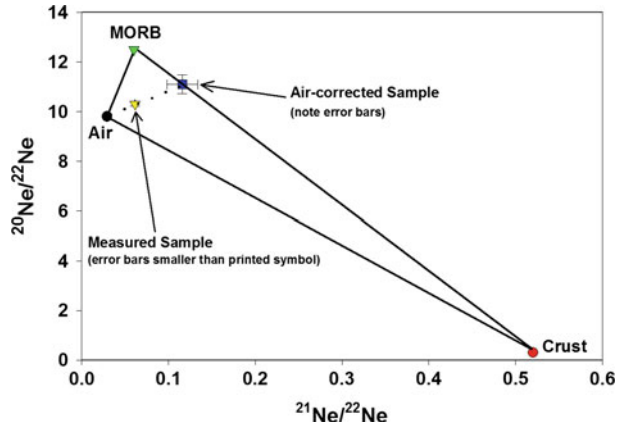

Fig. 5 Plot of $^{20}Ne/^{22}Ne$ against $^{21}Ne/^{22}Ne$ illustrating the three distinct sources of Ne in natural gas reservoirs (redrawn from Ballentine 1997). As the three end member ratios are known it is simple to correct any sample for atmosphere, crust or mantle contributions, taking due account of the error propagation. Example shows correction for the atmospheric contribution. The same procedure can be used for correction of crust and mantle contributions

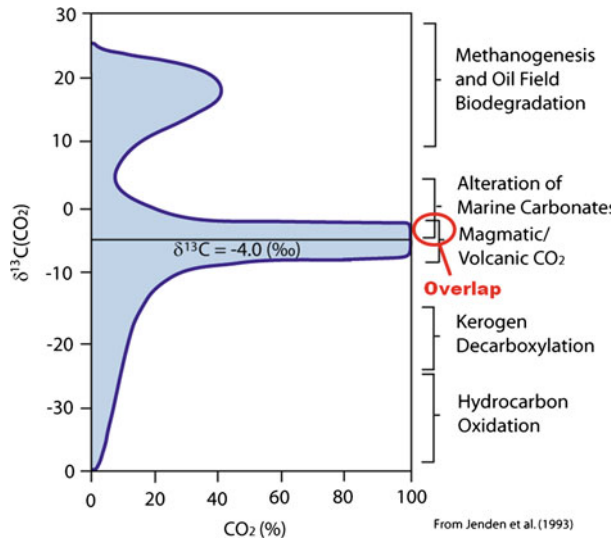

Fig. 6 Plot of CO_2 concentration against the range of $\delta^{13}C$ (%) observed in natural systems. The range of $\delta^{13}C$ values corresponding to a variety of natural processes are also labelled as is the clear overlap in the range of values that exists between magmatic CO_2 and the alteration of marine carbonates. Significantly these are the only sources that can account for reservoirs with high concentrations of CO_2

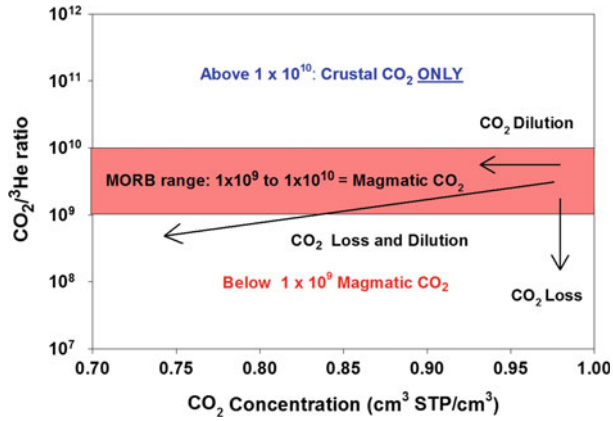

Fig. 7 Plot of CO_2 concentration against $CO_2/^3He$ ratio. The range of $CO_2/^3He$ values exhibited by mid-ocean ridge (MORB) popping rocks is highlighted by the *shaded* region. Any CO_2 that plot within or below this range, must contain a significant quantity of magmatic ^3He, implying a mantle origin for the CO_2. As the crust contains no ^3He, gases sourced from the crust have $CO_2/^3He$ values that plot above the shaded region (Ballentine et al. 2001, 2002; Sherwood Lollar et al. 1999; Zhou et al. 2005)

5 Use of Noble Gases in Natural CO_2 Reservoirs: Colorado Plateau, USA

The study of noble gases in the understanding of water—CO_2—oil interactions is still in the early stages but in principle, noble gases and the combination of noble gases and stable isotope data can provide a quantitative tool for tracing the processes occurring in the hydrogeological system that have direct relevance for long term carbon sequestration.

5.1 Determining the Source and Residence Time of CO_2

Noble gases have been particularly effective in determining the source of CO_2 within natural CO_2 reservoirs. Comparing the concentration of ^3He with the concentration of ^4He (i.e. the $^3He/^4He$ ratio) can identify magmatic contributions to subsurface reservoirs (Ballentine et al. 2002). In a similar fashion, the concentration of ^3He can be compared to the concentration of CO_2 within a natural CO_2 reservoir to determine the origin of the CO_2 (Marty et al. 1992; Oxburgh et al. 1986). Magmatic $CO_2/^3He$ ratios exhibit a small range when compared to other crustal fluids (1×10^9 to 1×10^{10}) (Ballentine et al. 2001) and hence can be used to identify and quantify the amount of mantle CO_2 in a particular reservoir.

Using this technique it has been established that five reservoirs (McCallum Dome, Sheep Mountain, McElmo Dome, Bravo Dome, St Johns Dome) surrounding the Colorado Plateau uplift region of the southwest U.S. primarily contain mantle-derived CO_2 (Fig. 8). Radiometric dating of surface volcanics surrounding these natural CO_2 reservoirs gives an indication of the approximate timing of CO_2 injection. The most recent magmatic event related to the natural CO_2 reservoirs investigated occurred at the Raton-Clayton volcanic field close to Bravo Dome between 10 and 8 ka (Broadhead 1998). The next youngest event is associated with St. Johns Dome, where the last phase of volcanic activity from the nearby Springerville Volcanic field dates from 0.3 to 2.1 Ma (Rauzi 1999). Magmatic activity associated with both the Sheep Mountain and McCallum Dome CO_2 reservoirs occurred in the Late Tertiary (Maughan 1988; Woodward 1983). The oldest intrusive igneous rocks close to a natural CO_2 reservoir are those associated with McElmo Dome, from the nearby Ute Mountain and La Plata Mountain laccoliths which have been dated

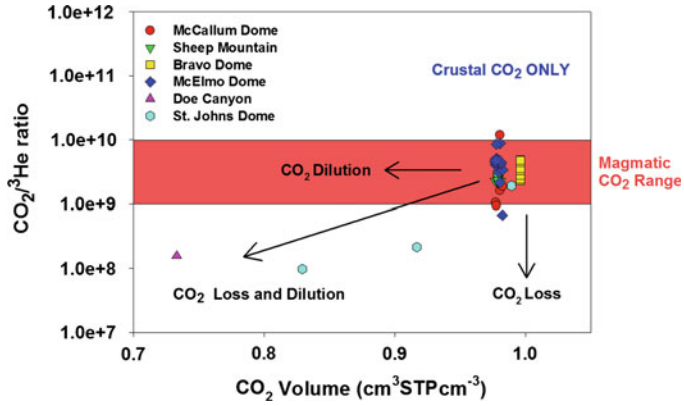

Fig. 8 Plot of $CO_2/^3He$ against CO_2 concentration for all of the reservoirs studied. All error bars are smaller than printed symbols. The *shaded region* highlights the range of $CO_2/^3He$ values measured in pure magmatic samples (MORB). All of the samples from the deep gas fields plot within or below this range, indicating the presence of a significant quantity of magmatic ^3He, implying a mantle origin for the CO_2 within these fields (Gilfillan et al. 2008). Doe Canyon is a small natural CO_2 reservoir related to McElmo Dome

at 40–72 Ma (Stevens et al. 2006). Whilst these ages were determined on surface intrusive igneous rocks, and it is probable that deep igneous activity will have continued for a significant period after these surface rocks were formed, it is clear that several of the natural reservoirs appear to have stored CO_2 for at least a million years. Indeed in two reservoirs CO_2 has been stored for considerably longer, namely McElmo Dome where CO_2 was injected ~40 million years ago (Gilfillan et al. 2008) and in the JM Brown Basset Field which is believed to have contained CO_2 for some 300 million years (Ballentine et al. 2001). In all these fields, $CO_2/^3He$ data show a magmatic origin for the CO_2 gases with evidence of CO_2 depletion relative to ^3He (Fig. 8).

5.2 Determining the Long Term Fate of CO_2

In addition to identifying the source of CO_2, noble gases can also be used to determine the long term fate of natural CO_2. Measured $CO_2/^3He$ ratios from nine CO_2 reservoirs from around the world (specifically the U.S., Europe and China) show a marked decrease in $CO_2/^3He$ ratios with increasing ^4He, (Fig. 9a) and where measured, ^{20}Ne (Gilfillan et al. 2009) (Fig. 9b). As ^3He is almost solely derived from the mantle, there is no source in the shallow crust that could increase its concentration after the premixed CO_2 and ^3He has entered the reservoir. Hence, the reduction in $CO_2/^3He$ can only be explained if the CO_2 component is being reduced relative to ^3He.

Due to its atmospheric origin, ^{20}Ne is a tracer of formation water interaction in crustal fluids. ^4He is a tracer of radiogenic input to a crustal fluid system, and accumulates in the formation water over time (hence its use for formation water dating). Therefore, the correlation between the $CO_2/^3He$ reduction and increasing ^{20}Ne and ^4He concentrations illustrates that contact with the formation water is directly controlling the removal of the CO_2 component in the natural CO_2 reservoirs.

5.2.1 Using Noble Gases and Carbon Isotopes to Identify Long Term Fate of CO_2

In each individual field, the reduction in $CO_2/^3He$ ratios allows the amount of CO_2 lost relative to ^3He to be calculated. Several of the reservoirs show an excess of 90 % loss of CO_2 compared to the highest $CO_2/^3He$ ratio measured (Gilfillan et al. 2009). Using stable carbon isotopes in conjunction with noble gas data it is

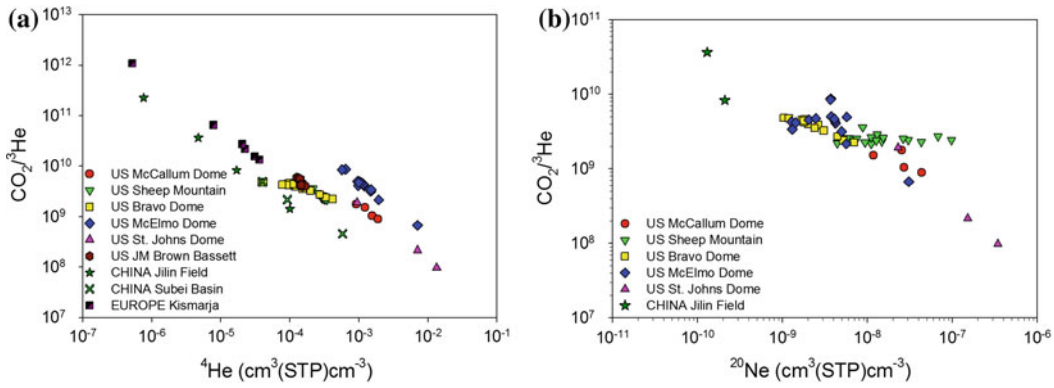

Fig. 9 **a** CO_2-rich gas fields from around the world also show a strong correlation between decreasing $CO_2/^3He$ and increasing ^4He concentrations. ^4He accumulates in the formation water over time and further indicates the importance of formation water in controlling the mechanism of subsurface CO_2 removal (Gilfillan et al. 2009). **b** $CO_2/^3He$ variation plotted against ^{20}Ne in samples from natural CO_2 reservoirs from around the world. There is a general trend in this data set of decreasing $CO_2/^3He$ with increasing ^{20}Ne. ^3He is conservative within the gas phase. Variations in $CO_2/^3He$ therefore represent subsurface removal of CO_2 from the emplaced CO_2 phase. As the only subsurface source of the ^{20}Ne which is now in the CO_2 phase is the formation water, the sink that is reducing CO_2 must be linked to the formation water which is in contact with the CO_2 (Gilfillan et al. 2009)

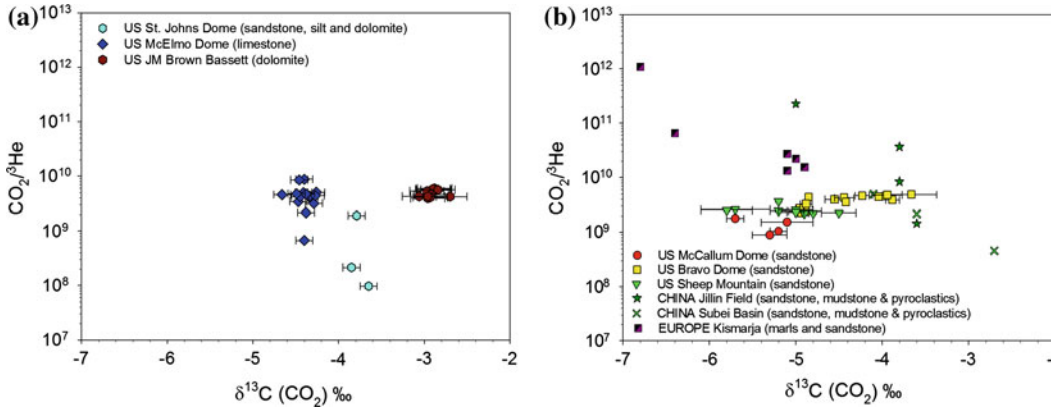

Fig. 10 Plot of $CO_2/^3He$ against $\delta^{13}C$ (CO_2) for all of the reservoirs in the study. The carbonate dominated reservoirs exhibit very little variation in $\delta^{13}C$ (CO_2) value, both within the individual reservoirs and between different reservoirs (*left*). The reservoirs which had a predominantly siliciclastic lithologies reservoirs exhibited a wider range of $\delta^{13}C$ (CO_2) values within and between the reservoirs (*right*) (Gilfillan et al. 2009)

possible to determine how much of this CO_2 component is being lost by dissolution into the formation water or by precipitation of new carbonate minerals. This is because precipitation of new carbonate minerals is a chemical process which strongly alters the $\delta^{13}C$ (CO_2) isotope values as a result of the preferential incorporation of ^{13}C in the precipitate. As both ^{12}C and ^{13}C have similar solubility, dissolution of CO_2 into the formation water has a lesser effect on the $\delta^{13}C$ (CO_2) isotope values, although this is also pH dependent.

All of the natural CO_2 reservoirs investigated exhibited a small range of carbon isotope values, despite large reductions in the CO_2 component relative to ^3He. This shows that the majority of the CO_2 is being removed by dissolution into the formation water. Individual reservoir lithologies

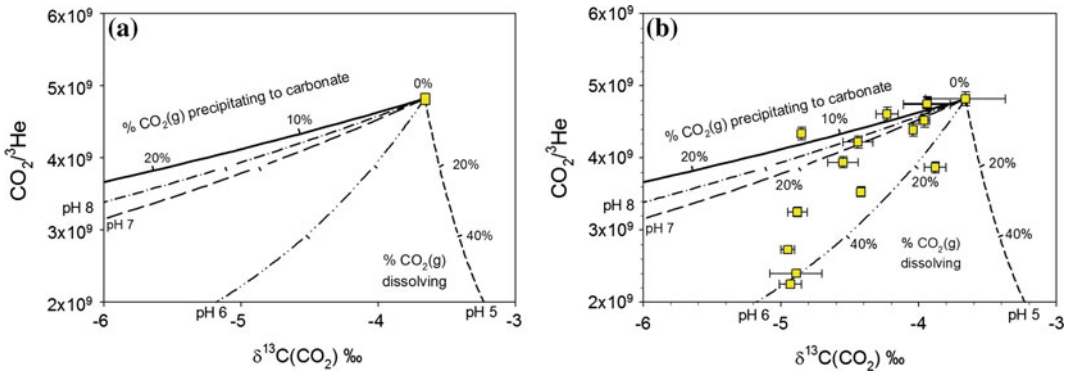

Fig. 11 **a** Model of evolution of gas phase $CO_2/^3He$ ratio and $\delta^{13}C$ of the CO_2 under Bravo Dome reservoir conditions. Using a combination of noble gas and $\delta^{13}C(CO_2)$ stable isotopes determination and quantification of the different mechanisms of CO_2 removal from natural CO_2 reservoirs is possible. This is because $\delta^{13}C(CO_2)$, the stable carbon isotope value of the residual CO_2 phase, is changed, or 'fractionated', by different amounts depending on the loss mechanism. Specifically, precipitation of CO_2 as carbonate minerals has a distinct fractionation from CO_2 dissolving to into the formation water in the reservoir. **b** Plot of $\delta^{13}C(CO_2)$ against $CO_2/^3He$ for the siliciclastic Bravo Dome field as CO_2 gas is either dissolved under different pH (*dashed lines*) or precipitated in an open system by Rayleigh fractionation (*solid line*). The Bravo Dome samples exhibit up to 18 % CO_2 loss by carbonate precipitation and up to 60 % dissolved into the formation water (Gilfillan et al. 2009)

exhibited a clear control on the variation of $\delta^{13}C$ (CO_2) isotopes both within and between the individual natural reservoirs. Within the carbonate dominated reservoirs very little variation in $\delta^{13}C$ (CO_2) values is observed compared to the much wider range of values which were exhibited in the siliciclastic dominated reservoirs (Fig. 10).

Evidence to suggest that precipitation of new carbonate minerals is responsible for some reduction of the CO_2 component is found only in sandstone-dominated reservoirs. This was particularly the case in the Bravo Dome CO_2 reservoir, where the measured values for one sample indicated that up to 18 % of the CO_2 component could have been precipitated (Fig. 11). The dataset from Sheep Mountain indicates that a maximum of 10 % of the CO_2 could have also have been removed by precipitation (Fig. 12a). However, the remaining four siliciclastic and all three of the carbonate dominated reservoirs, such as McElmo Dome (Fig. 12b) showed very little evidence of precipitation and it is clear that CO_2 dissolution into the formation water is the only significant CO_2 sink over geological timescales (Gilfillan et al. 2009).

5.2.2 Using Noble Gases and Carbon Isotopes to Determine Reservoir pH Conditions

Combining the $CO_2/^3He$ ratio reduction with the corresponding fractionation of the $\delta^{13}C$ (CO_2) isotopes also permits determination of the reservoir pH conditions under which the CO_2 dissolution into the formation water is occurring (Fig. 11). This is the result of the different carbon stable isotope fractionation factors which act on CO_2 gas dissolving either to bicarbonate (HCO_3^-) or carbonic acid (H_2CO_3) (Deines et al. 1974). The proportion of CO_2 dissolving to each species is directly controlled by pH, meaning that the $\delta^{13}C$ (CO_2) fractionation trend can be used to determine the pH conditions under which dissolution is occurring (Fig. 11). This is a significant breakthrough in the understanding of natural CO_2 reservoir conditions, as subsurface pH measurements are notoriously difficult to obtain. As with $\delta^{13}C$ (CO_2) values, the reservoir lithology exhibits a clear control on the pH range observed in the different CO_2 reservoirs. A pH range of 5.0–5.3 was observed in the six siliciclastic reservoirs, compared to the higher values of 5.4 to 5.8 determined for the

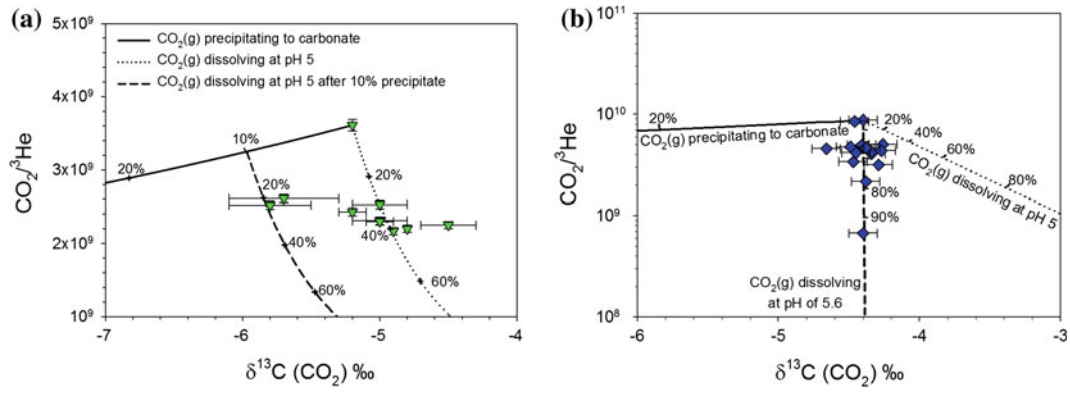

Fig. 12 **a** Plot of $\delta^{13}C$ (CO_2) against $CO_2/^3He$ for the siliciclastic Sheep Mountain field. Whilst the majority of the dataset is consistent with dissolution of CO_2(g) at pH = 5, a number of data points require approximately 10 % of the CO_2(g) precipitating as carbonate, together with dissolution of CO_2(g) into the formation water at a pH of = 5 in a two process model similar to that outlined for Bravo Dome. **b** Plot of $\delta^{13}C(CO_2)$ against $CO_2/^3He$ for the carbonate McElmo Dome field. This shows the relationship between $CO_2/^3He$ and $\delta^{13}C$ (CO_2) observed in the majority of the CO_2 reservoirs. This relationship indicates that the dominant CO_2 sink in these natural systems is dissolution into the formation water. Error bars represent analytical uncertainty on the measured data points

three carbonate reservoirs. This can be accounted for by the buffering capacity provided by additional bicarbonate ions which originate from the dissolution of carbonate minerals in the carbonate-dominated reservoirs. The pH ranges recorded in the natural reservoirs are also consistent with the subsurface pH value of 5.7 observed in the recent CO_2 injection experiment in the Frio formation in Texas (Kharaka et al. 2006).

5.3 Physical Chemistry of Dissolved Noble Gases

The different noble gas isotope systems can tell us about the different proportions of air or crustal derived noble gases within a reservoir but they cannot shed light on the physical processes that occur within these reservoirs. This is because processes such as degassing and phase interactions do not alter the isotopic compositions unless the timescales over which they occur are short than the noble gas diffusion rates. Therefore one must identify the relative solubilities of the noble gases to determine their complex histories within a reservoir, acknowledging that each reservoir will have unique physical conditions and therefore unique 'starting' compositions upon which physical processes leave their fractionating fingerprints. To begin with we must quantify noble gas solubilities in different phases under reservoir conditions to establish these initial noble gas compositions within a reservoir.

Fundamentally, the solubility of noble gases in solution is governed by Henry's law:

$$p_i = K_i x_i \tag{6}$$

where p_i is the partial pressure of gas i in equilibrium with a fluid containing x_i mole fraction of i in solution and K_i is Henry's constant.

Henry's coefficient varies with pressure, temperature and salinity of the fluid. However at the temperatures and pressures found in crustal fluid systems, empirical data are not available. Consequently the equation must be modified to include non-ideality in both the gas and liquid phase. The modified equation then becomes:

$$\phi_i p_i = \gamma_i K_i x_i \tag{7}$$

where Φ is the gas phase fugacity coefficient and γ is the liquid phase activity coefficient.

In the gas phase, the real molar volume can be calculated from:

$$PVm/RT = 1 + B(T)/V_m + C(T)/V_{m^2} \quad (8)$$

From which the fugacity coefficient can be derived via:

$$\Phi(P,T) = \exp[B(T)/V_m + (C(T) + B(T)^2/2V_{m^2} \quad (9)$$

Where P is the total pressure, R is the gas constant, T is the temperature and B(T) and C(T) the temperature dependant first and second order virial coefficients.

Non ideality in the liquid phase cannot be determined using equations of state because of the complexity of solute/solute and solvent/solute interactions. γ is considered to be independent of pressure therefore deviation from ideality caused by temperature and electrolyte concentration is assessed from empirically derived data. For a more extensive review of physical chemistry in liquid and gas phase see Ballentine and Burnard (2002).

5.4 Noble Gas Fractionation and Partitioning Between Phases

Of more direct relevance to assessment of subsurface CO_2 storage using noble gases, is the modelling of solubility fractionation between subsurface phases in open and closed systems (Ballentine et al. 1996; Hiyagon and Kennedy 1992; Pinti and Marty 1998; Torgersen and Kennedy 1999; Zartman et al. 1961). Noble gases alone can also be used to identify interactions between different fluid phases. In the simplest scenario, equilibration of a large gas/water volume ratio in the subsurface would be expected to cause near quantitative degassing of the formation water and result in a gas phase that inherits the formation water noble gas isotopic and elemental composition. This composition would be expected to be similar to the calculated air saturated water (ASW) noble gas composition, determined using appropriate recharge conditions (for the Bravo Dome field used as the example here an ASW $^{20}Ne/^{36}Ar$ of 0.152 was determined assuming air equilibration at 10 °C and a small excess air component of 10 % Ne (Kipfer et al. 2002). As the subsurface gas/water volume ratio decreases the least soluble gases will tend to be enriched in the gas phase until $V_{gas}/V_{water} \rightarrow 0$ when the limit of the enrichment is controlled by the relative solubility of the respective gases. For example, the maximum enrichment of the Ne relative to Ar in the gas phase though phase equilibrium degassing is K_{Ne}/K_{Ar} where K_{Ne} and K_{Ar} are the respective Henry's constants for Ne and Ar (e.g. Ballentine et al. 1991, 2002). K_{Ne} and K_{Ar} for average field conditions predict a maximum enrichment of Ne relative to Ar from ASW values by a factor of ~ 2 corresponding to a maximum $^{20}Ne/^{36}Ar$ of 0.304, which is significantly lower than the range of $^{20}Ne/^{36}Ar$ values (0.314–0.617) observed in the Bravo Dome dataset (Fig. 13). The Sheep Mountain data exhibits even more extreme $^{20}Ne/^{36}Ar$ values which range from 0.530 to 2.496. Clearly both datasets cannot be explained by simple equilibration between the CO_2 and formation water phases and must be explained by a more complex equilibration history.

5.4.1 Solubility Controlled Phase Fractionation

Henry's Law (Eq. 1) defines the fractionation between the gas phase and the liquid phase with which it is in equilibrium. Again assuming ideal gas behaviour, this can be rewritten to relate the concentration in the gas phase, C_g^i, to the concentration in the fluid phase, C_l^i, via Henry's constant K_l^d :

$$C_g^i = K_i^d C_l^i \quad (10)$$

The equilibrium concentrations are also dependent on the gas/liquid volume ratio (V_l/V_g), related by

$$[i]_g = [i]_T \left(V_l/V_g K_i^d + 1\right)^{-1} \quad (11)$$

Where $[i]_g$ is the number of moles in the gas phase and $[i]_T$ is the total number of moles. As

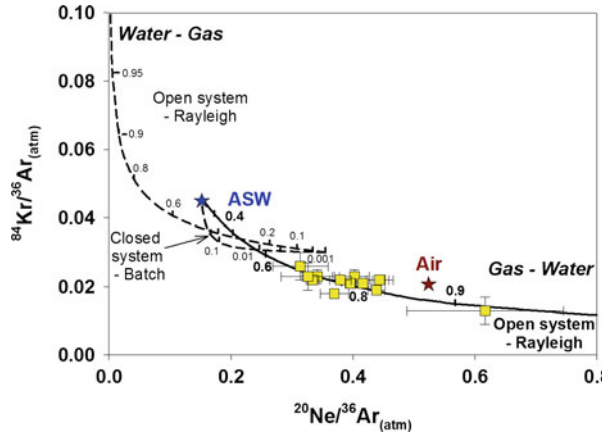

Fig. 13 Plot of $^{20}Ne/^{36}Ar_{(atm)}$ against $^{84}Kr/^{36}Ar_{(atm)}$ for the Bravo Dome field. Also plotted are the Air and ASW values and the calculated Rayleigh and Batch fractionation curves for a gas phase exsolving from a groundwater that has an initial ASW composition (Eq. 6) (*dashed lines*). The *tick marks* on the *dashed lines* represent the proportion of Ar remaining in the groundwater phase. Also plotted is the Rayleigh fractionation line (Eq. 15) which would be produced by a gas phase dissolving into a water phase initially containing no noble gases (*solid line*). This is the re-dissolution model discussed in the text (Eq. 17). The *bold tick marks* on the solid fractionation line represent the proportion of Ar *lost* from the gas phase. The fractionation pattern observed in the air derived ratios can be explained by the re-dissolution model (Gilfillan et al. 2008)

$V_l/V_g \rightarrow 0$, $[i]_g \rightarrow [i]_T$. Giving Henry's constant units of molality leads to:

$$A_g = A_r \left[\frac{22400 T \rho_1 V_1}{1,000 \times 273 \frac{\gamma_A}{\phi_A} K_i^m V_g} + 1 \right]^{-1} \quad (12)$$

where:

A	number of moles
ρl	the density of the liquid l (g/cm^3)
T	Temperature
Vl, g	Volume of liquid l, or gas g in cm^3
Ki^m	Henry's constant (Kg atm/mol)

This determines the partitioning between the gas and liquid phase and makes it possible to calculate the volume of gas with which a liquid has equilibrated by using only one noble gas concentration in the liquid phase. This method assumes that during each stage of degassing, V_{gas}/V_{water} is small and by iteratively equilibrating small volumes of gas with progressively degassed groundwater, one can calculate the number of single stage equilibration episodes that must have occurred to produce an observed loss of the noble gas in question. Summing the volumes of gas defines the total of volume of gas exsolved from the groundwater, hence the gas/groundwater volume ratio (e.g. Zhou et al. 2005).

In practice it is often difficult to assess the initial concentrations of noble gases observed in the liquid phase. In this case, the relative fractionation between two different noble gases can be employed to determine the extent of fractionation processing.

$$\left(\frac{A}{B}\right)_{gas} = \left(\frac{A}{B}\right)_{groundwater} \frac{\left(\frac{Vg}{Vl} + \frac{1}{K_B}\right)}{\left(\frac{Vg}{Vl} + \frac{1}{K_A}\right)} \quad (13)$$

as

$$\text{as } \frac{Vg}{Vl} \rightarrow 0, \frac{\left(\frac{A}{B}\right)_{gas}}{\left(\frac{A}{B}\right)_{groundwater}} \rightarrow \frac{\frac{rA}{\phi A} K_A}{\frac{rA}{\phi B} K_B} = \alpha \quad (14)$$

Where:

$\left(\frac{A}{B}\right)_{groundwater}$	$\frac{A}{B}$ original groundwater ratio and A & B are different noble gases
$\left(\frac{A}{B}\right)_{gas}$	$\frac{A}{B}$ ratio in the gas phase

α	Fractionation coefficient calculated for the gas/groundwater system
K_A, K_B	Henry's constants for gases A and B
r_A, r_B	Groundwater phase activity coefficients
ϕ_A ϕ_B	Gas phase fugacity coefficients

5.4.2 Rayleigh Fractionation (Open System)

Noble gas partitioning from a water phase into a gas phase (degassing) can also follow the Rayleigh fractionation law, provided that the gas phase is continually removed. Rayleigh fractionation can be expressed as:

$$\left(\frac{A}{B}\right)_{groundwater} = \left(\frac{A}{B}\right)_0 f^{\alpha-1} \quad (15)$$

$$\alpha = \frac{\frac{rA}{\phi A} K_A^{groundwater}}{\frac{rA}{\phi B} K_B^{groundwater}} \quad (16)$$

Where:

$\left(\frac{A}{B}\right)_{groundwater}$	$\frac{A}{B}$ ratio in the groundwater and A and B are different noble gases
$\left(\frac{A}{B}\right)_0$	The original groundwater phase $\frac{A}{B}$ ratio
f	Fraction of B remaining in the groundwater phase

Equally, one may also consider the opposite situation, in which noble gases in the gas phase are re-dissolved into groundwater that has been previously stripped of noble gases, as might occur during contact with a CO_2 phase. In this case, the ratio A/B will evolve in the opposite direction, given by:

$$\left(\frac{A}{B}\right)_{groundwater} = \left(\frac{A}{B}\right)_0 f^{\left(\frac{1}{\alpha}-1\right)} \quad (17)$$

In principle, multiple stages of exsolution and dissolution could increase the magnitude of fractionation in a gas phase over that predicted by the phase equilibrium model limit (Zartman et al. 1961). In this case a gas phase exsolved from the water with a low gas/water volume ratio will have an elevated $^{20}Ne/^{36}Ar$ ratio. This could be re-dissolved into a smaller volume of water by a change in physical conditions such as a pressure increase, a decrease in temperature and salinity, or mixing with unsaturated (with respect to the gas phase) water. This would create a local increase in both the formation water noble gas concentration and the magnitude of noble gas fractionation in solution. Subsequent formation of a gas phase in equilibrium with the now modified formation water could result in a fractionation significantly in excess of that predicted by the single stage equilibrium model. For this process to occur the pressure/temperature conditions must fluctuate, and the resulting fractionated gas phase volume must be very small compared to the fluid/water volume required to produce significant fractionation (Ballentine et al. 2002). This is unlikely to have occurred on a gas field scale so it can be discounted as a viable mechanism to account for the extreme values observed in the Bravo Dome and Sheep Mountain datasets.

A second possible mechanism considered is non-equilibrium diffusion. Torgersen et al. (2004) have proposed that variable enrichments of noble gases can be accounted for by incomplete emptying followed by partial filling of lithic grains and half spaces, similar to the mechanism proposed by Pinti et al. (1999) for air diffusion into fresh pumice. They further demonstrate that both elemental and isotopic compositions of Ne and Ar show clear mass-dependent fractionation (Pinti et al. 1999). Whilst the significant mantle and crustal Ne contributions to the Colorado Plateau reservoirs makes subtle isotopic fractionation in Ne hard to identify, no significant mass-dependent fractionation in either the $^{38}Ar/^{36}Ar$ ratios or elemental abundance patterns was observed meaning that non-equilibrium diffusion could be ruled out (Holland and Ballentine 2006).

Another mechanism which could account for the extreme $^{20}Ne/^{36}Ar$ fractionation is interaction of the gas with an oil phase. This is because Ar (and also Kr and Xe), relative to Ne, is more soluble in oil than water meaning that

equilibration of the groundwater with an oil phase could increase the $^{20}Ne/^{36}Ar$ of the water phase (Bosch and Mazor 1988). Subsequent degassing of the groundwater into the gas phase could then result in higher $^{20}Ne/^{36}Ar$ ratios in the gas. This has been suggested as an explanation for elevated $^{20}Ne/^{36}Ar$ ratios measured in the Indus Basin, Pakistan (Battani et al. 2000) and Mexico gas fields (Sarda et al. 2000), where the term double-distillation is used. However, there is no evidence of significant hydrocarbon components in the Bravo Dome CO_2 field and hence, oil interaction can be discounted as a valid explanation of the high $^{20}Ne/^{36}Ar$ ratios. Additionally, in the Indus study there is a correlation between the $^{20}Ne/^{36}Ar$ and $1/^{36}Ar$ ratios but no such correlation exists in the Bravo Dome or Sheep Mountain datasets.

Having ruled out the above mechanisms, a more appropriate model must be devised to explain the high $^{20}Ne/^{36}Ar$ ratios observed in the Colorado Plateau CO_2 reservoirs. One such model is a two stage partial re-dissolution model (Gilfillan et al. 2008). The preservation in some samples near ASW ratios suggests that some degree of 'gas stripping' of the formation water noble gas composition has occurred with complete removal of noble gases into the gas phase. Stage one involves such a complete degassing to provide an ASW starting composition for stage II, which consists of Rayleigh fractionation (open system) of the noble gases from the gas phase into the noble gas stripped formation water (potentially as a result of stage 1).

Neither closed system batch fractionation nor open system Rayleigh degassing models of gas exsolving from an ASW groundwater phase can account for the observed maximum fractionation of $^{20}Ne/^{36}Ar_{(atm)}$ and $^{84}Kr/^{36}Ar_{(atm)}$ in the Bravo Dome reservoir (Fig. 13). The values can however, be explained by the re-dissolution model. It is proposed that gas stripping of the reservoir formation water occurs during the injection and movement of magmatic CO_2 through the formation water during the initial reservoir filling stage. This is corroborated by the orders of magnitude lower ^{20}Ne concentration in the gas phase than that predicted by groundwater degassing (Fig. 14). The CO_2 migrates as a separate phase and as it is an excellent solvent, would have had the capacity to quantitatively partition any gases from the water phase into the CO_2, effectively 'stripping' the formation water of its dissolved gas content. This will produce a CO_2 reservoir with an ASW-like composition which will also have incorporated any radiogenic-crustal noble gases that had previously accumulated in the formation water. At this stage the formation water will be saturated with respect to CO_2, but completely depleted with respect to the atmosphere-derived noble gases.

In the Bravo Dome system, coherent fractionation of the crustal radiogenic and formation water-derived noble gases indicates that the formation water and CO_2 were well mixed prior to the fractionation occurring, hence the fractionation process must have occurred after the ASW gas stripping. Subsequent charges of magmatic CO_2 would then pass through the gas stripped formation water but will only dilute the ASW-derived and crustal-radiogenic noble gases in the CO_2 trapping structure. Bravo Dome preserves a clear ^{20}Ne concentration gradient, increasing from west to east in the field. It is argued this both corroborates the model and indicates the reservoir filling direction, which may still be ongoing, to be from the west (Baines and Worden 2004b).

Following reservoir filling the noble gases now in the CO_2 phase will then re-equilibrate with the degassed formation water. This re-equilibration will occur under either open system or closed system conditions depending on the available volume of water for re-equilibration and if there is significant water migration or recharge. For open system conditions, the re-dissolution process will follow a Rayleigh fractionation path. Under closed system conditions, the trend will be the exact reverse of that calculated for batch fractionation of a gas phase exsolving from water. Under the Bravo Dome reservoir conditions, the open system Rayleigh fractionation re-dissolution model accounts for all of the mantle corrected $^{20}Ne/^{36}Ar_{(atm)}$ and $^{84}Kr/^{36}Ar_{(atm)}$ ratios that are observed in the field (Fig. 13). The conceptual model is also

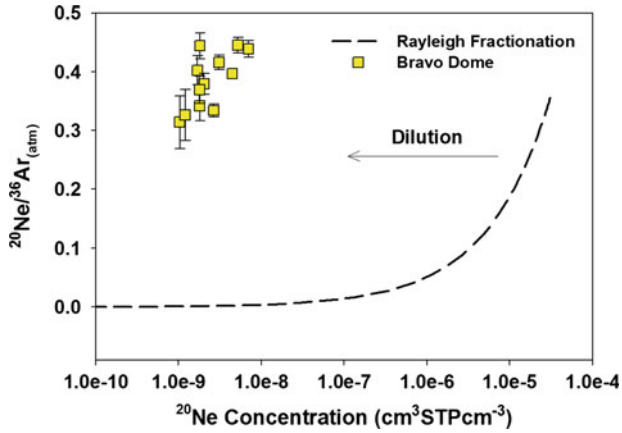

Fig. 14 Plot of $^{20}Ne/^{36}Ar_{(atm)}$ against $^{20}Ne_{(atm)}$ for the samples from the Bravo Dome field. Also plotted are the predicted ^{20}Ne concentration values assuming Rayleigh Fractionation of a gas phase exsolving from the groundwater. The predicted concentrations are several orders of magnitude greater than the observed concentrations, implying that the atmospheric noble gases within the reservoir have been significantly diluted, most probably by injection of magmatic CO_2

presented as a cartoon (Fig. 15) from Gilfillan et al. (2008).

5.4.3 Quantifying the Extent of Water Interaction

Using the open system re-dissolution model outlined above, the fractionation of the measured gas phase $^{20}Ne/^{36}Ar$ ratios from the initial ASW formation water value can be used to define the proportion of ^{36}Ar lost from the gas phase into solution. Using this value it is then straightforward to calculate the initial concentration of ^{36}Ar, $^{36}Ar_{init}$, within the gas phase prior to the re-dissolution process (Zhou et al. 2005). Using the concentration of ^{36}Ar in ASW it is then possible to calculate, for each sample, the volume of water required to have been gas 'stripped' to supply the $^{36}Ar_{init}$ to provide the Stage 1 Water/Gas volume ratio. For Bravo Dome system, Stage 1 Water/Gas volume ratio ranges from 0.0005 to 0.071 cm^3 of water per cm^3 gas (STP) (Table 3). Under reservoir conditions 1 cm^3 of groundwater can hold 4.66 cm^3 of CO_2 (STP) in solution (Spycher and Pruess 2005). This results in a water/gas ratio of 0.215 and is far higher than the largest estimated Stage 1 V_{Water}/V_{Gas} Bravo Dome value. This is consistent with the CO_2 gas charging the reservoir as a separate and distinct phase, and hence is consistent with the proposed CO_2 'stripping' of the formation model (Fig. 15).

One can then calculate the volume of water, under reservoir conditions (Table 3), that the noble gases of the CO_2 phase must re-dissolve into, in order to fractionate the $^{20}Ne/^{36}Ar$ values from ASW (0.152) to the values observed. For the Bravo Dome reservoir these vary from 0 to 104 cm^3 water per cm^3 gas (RTP) (RTP = Reservoir Temperature and Pressure), which corresponds to 0–1.51 cm^3 water per cm^3 gas (STP). The volume of degassed water required to fractionate the $^{20}Ne/^{36}Ar$ from ASW to observed values is far larger than the volume of water 'stripped' to supply the gases, by up to a factor of 50. Little, if any, CO_2 will dissolve in this water while it remains CO_2 saturated. This analytical technique is able to quantify on a sample by sample basis the volume of water the CO_2 in this storage analogue has interacted with both (1) on reservoir filling; and (2) subsequent to reservoir filling.

5.4.4 Adsorptive Fractionation

Several studies have suggested that physical fractionation processes such as adsorption can result in a relative gas abundance pattern that is

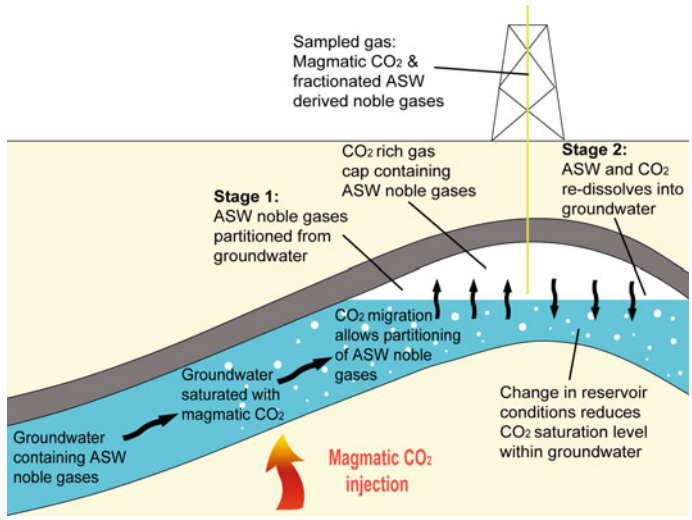

Fig. 15 Cartoon illustrating the two stage degassed formation water and re-dissolution model. *Stage 1*: Magmatic CO_2 injection into the formation water causes the water to become fully saturated in CO_2, with excess gas forming a free CO_2 phase. The free CO_2 phase migrates upwards, stripping dissolved air-derived noble gases and accumulated crustal/radiogenic noble gases as it does so. This results in formation water which is fully saturated in CO_2 and completely degassed with respect to ASW and crustal derived noble gases (and N_2). When this CO_2 containing the noble gases stripped from the formation water encounters a trapping structure, it provides the first reservoir fluid charge. Subsequent charges of CO_2 provide no more ASW and crustal noble gases, and serve only to dilute the original ASW and crustal noble gas rich CO_2. Reservoir scale preservation of concentration gradients in ASW-derived noble gases therefore provide an indication of CO_2 filling direction (cf Bravo Dome, St Johns). *Stage 2*: When recharge of the CO_2 cap stops, the noble gases begin to re-dissolve into the gas stripped groundwater. This results in a fractionation of the ASW-derived noble gases. The magnitude of this fractionation depends on the volume of water in contact with the gas phase and whether open or closed system fractionation conditions are present. Hence, only limited CO_2 re-dissolution can, and only as result of a change in reservoir conditions or CO_2 precipitation as new carbonate minerals causing a reduction of the CO_2 saturation level of the formation water. Figure reproduced from Gilfillan et al. (2008)

highly enriched in heavy noble gas isotopes (Kr and Xe). $^{130}Xe/^{36}Ar$ enrichment factors up to ~600 relative to air and ~200 relative to water in equilibrium with air having been observed. (Fanale and Cannon 1971; Kennedy et al. 1990, 2002; Torgersen et al. 2004). These components cannot be directly determined from ASW by distillation or re-equilibration with oil, gas or oil–gas systems and thus require desorption of these gases from organic matter into fluids (Kennedy et al. 2002; Torgersen and Kennedy 1999). Evidence for this hypothesis is provided by the fact that large quantities of Xe can be adsorbed onto carbon-rich materials at room temperature (Fanale and Cannon 1971; Podosek 1980). Recent work by Torgersen et al. (2004) has reported that these enrichments of noble gases could be accounted for by incomplete emptying followed by incomplete filling of lithic grains and half spaces.

5.4.5 Diffusive Fractionation

Maximum diffusive fractionation will occur under non-equilibrium conditions when the different diffusion properties of the noble gases and CO_2 control the partitioning rate from water into the gas phase. The fractionation or diffusion coefficient of a ratio A/B can be calculated using the Graham's law of diffusion:

$$\alpha_{\frac{A}{B}} = \sqrt{\frac{M_B}{M_A}} \tag{18}$$

where:

A and B	Isotopes
M_A, M_B	Mass of A and B

Table 3 Calculated formation water noble gas concentrations (cm^3STPcm^{-3}) and ratios (Gilfillan et al. 2008)

Field and well	Observed $^{20}Ne/^{36}Ar$	Proportion ^{36}Ar lost to stage 2 water	Measured ^{36}Ar $cm^3(STP)cm^{-3}$ ($\times 10^{-8}$)	$^{36}Ar_{init}$ $cm^3(STP)cm^{-3}$ ($\times 10^{-8}$)	Stage 1 V_{water}/V_{Gas} (STP)	Stage 2 V_{water}/V_{Gas} (STP)	Stage2 V_{water}/V_{Gas} (RTP)
Bravo Dome							
BD01	0.362	0.786	0.212	0.992	0.0090	1.261	87.01
BD02	0.426	0.841	1.25	7.87	0.0714	1.502	103.60
BD03	0.430	0.843	0.881	5.62	0.0510	1.513	104.39
BD04	0.406	0.826	0.222	1.27	0.0115	1.429	98.57
BD05	0.385	0.809	0.873	4.56	0.0414	1.351	93.24
BD06	0.349	0.772	0.299	1.31	0.0119	1.206	83.23
BD07	0.279	0.661	0.191	0.562	0.0051	0.883	60.95
BD08	0.314	0.726	0.505	1.84	0.0167	1.057	72.94
BD09							0.00
BD10	0.395	0.818	0.499	2.73	0.0248	1.389	95.83
BD11	0.152	0.00	0.0549	0.0547	0.0005		0.00
BD12							0.00
BD13	0.347	0.770	0.406	1.76	0.0160	1.199	82.73
BD14	0.296	0.695	0.290	0.948	0.0086	0.969	66.86
BD12b	0.430	0.843	0.0494	0.315	0.0029	1.513	104.39

Hence, for the $^{20}Ne/^{36}Ar$ ratio $\alpha = 1.34$, and for the $^{84}Kr/^{36}Ar$ system $\alpha = 0.655$. As these values depend on the relative mass of the noble gas species, they are independent of the individual reservoir conditions. While some natural gas reservoirs show evidence of isotopic fractionation by diffusion (Zhou et al. 2005) others do not (Holland and Ballentine 2006; Holland et al. 2009).

6 Use of Noble Gases in Hydrocarbon Fields Relevant to CO_2 Storage

6.1 Tracing of CO_2 Injected for EOR, Mabee Oil Field Texas

Noble gas tracing has been used successfully for large-volume groundwater tracing in several different locations (Castro and Goblet 2003; Castro et al. 1998). Nimz and Hudson (2005) undertook an investigation to determine whether noble gases could also be used for CO_2 tracing. This study involved an analysis of noble gas tracer costs, availability, detection limits, and a comparison with other potential tracers.

At the time of the study no CO_2 storage operations were being conducted in which a noble gas tracer could be added therefore the work was undertaken at an active EOR location, the Mabee Oil field in Texas. Fortunately, the CO_2 being injected into the subsurface in the Permian Basin of West Texas contains unique and readily identifiable noble gas isotopic characteristics as the CO_2 originates from the extensive CO_2 reservoirs from the Colorado Plateau region previously discussed in this chapter. This CO_2 is transported via pipelines to West Texas. Therefore, Nimz and Hudson did not have to artificially add noble gases to the CO_2 stream and wait months or years for them to arrive at monitoring wells, they simply investigated the noble gas composition of the producing wells at the field.

Nimz and Hudson collected CO_2 from the pipeline prior to it being injected in the oil field and produced gases from 13 producing oil wells in the Mabee field. The gases extracted from all the Mabee field wells is collected and combined into a single pipeline and which is then mixed

with incoming 'fresh' Colorado Plateau CO_2 and re-injected into the field. This 'blend' of CO_2 was also collected for noble gas analysis. This allowed comparison of the isotopic composition of the injected CO_2 with the CO_2 produced from wells a significant distance from the original injection point. This provided an excellent analogue of tracing in an engineered storage site where noble gases could be injected along with CO_2 and then their distribution could be monitored through outlying wells. It should be noted that the concentrations of noble gases in the injected natural CO_2 from the Colorado Plateau reservoirs is significantly lower than those that would arise from the addition of a spike of artificial noble gases, meaning the study represents a much more difficult monitoring situation than would arise in an engineered storage site.

The wells sampled are shown in Fig. 16, along with the wells that were injecting CO_2 during the period of sampling. As injection had been taking place for many years, the entire field has been subject to injected CO_2 flood.

Nimz and Hudson found that the incoming CO_2 ($KMCO_2$) was isotopically similar to the CO_2 found in McElmo Dome, indicating that the majority of the CO_2 injected into the Mabee field at the time of the study was from McElmo Dome (Fig. 17a). This was somewhat surprising for two reasons; firstly as the operators of the field thought they were receiving CO_2 from Bravo Dome and secondly as there are several CO_2 fields that feed the CO_2 pipeline and hence a more mixed noble gas composition was expected.

Compared to $KMCO_2$ the Mabee production wells all exhibited more 'air like' noble gas composition. This was thought to be the result of either the baseline oil reservoir composition (present prior to CO_2 injection commencing) or from the large amount of water that is also injected into the field with CO_2. (This is because EOR operation in Mabee is a water alternating gas/CO_2 type (WAG), where water and CO_2 are injected into the field at separate times). It was possible to rule out atmospheric contamination during sampling as a cause of this component as the $^{20}Ne/^{36}Ar$ trend recorded from the samples

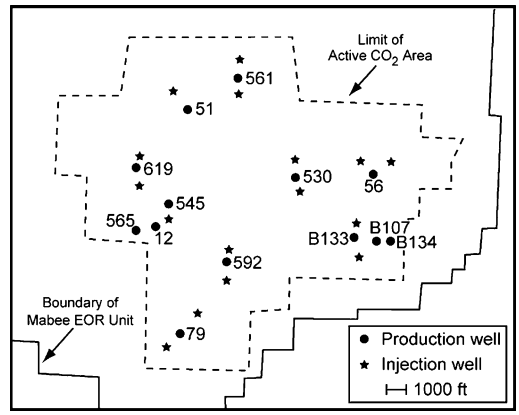

Fig. 16 Map of the southern portion of the Mabee EOR field. The production wells that Nimz and Hudson sampled are shown with adjacent sample numbers. The injection wells shown are those that were known to be active during the sampling period. There are numerous other production wells which are not shown, these occur on approximately 1,000 ft spacings (Nimz and Hudson 2005)

was not close to the fractionation trend expected if the injected $KMCO_2$ was in contact with the atmosphere (Fig. 17c). Instead the samples plotted close to the expected fractionation which would occur if the $KMCO_2$ was in contact with air saturated water (ASW), indicating that the injected water in the field had a strong influence on the noble gas composition of the samples.

From Fig. 17 it is apparent that an additional component must be present in the ASW component because a clear excess in crustal radiogenic ^{40}Ar and nucleogenic ^{21}Ne relative to the predominantly air-derived ^{36}Ar and ^{20}Ne was recorded. This excess component can be clearly seen in Fig. 17b as the trend exhibited by the Mabee samples toward a position with elevated ^{40}Ar relative to excess ^{21}Ne. The radiogenic origin of ^{21}Ne and ^{40}Ar requires this additional component must be crustal in origin.

A similar crustal component was observed in the Xe isotope composition. The samples were found to be enriched in crustal radiogenic $^{132-136}Xe$ relative to atmosphere derived ^{130}Xe. Figure 18d illustrates this excess ^{132}Xe relative to the ASW and air fractionation trends. Unfortunately it was not possible to collect a sample of the

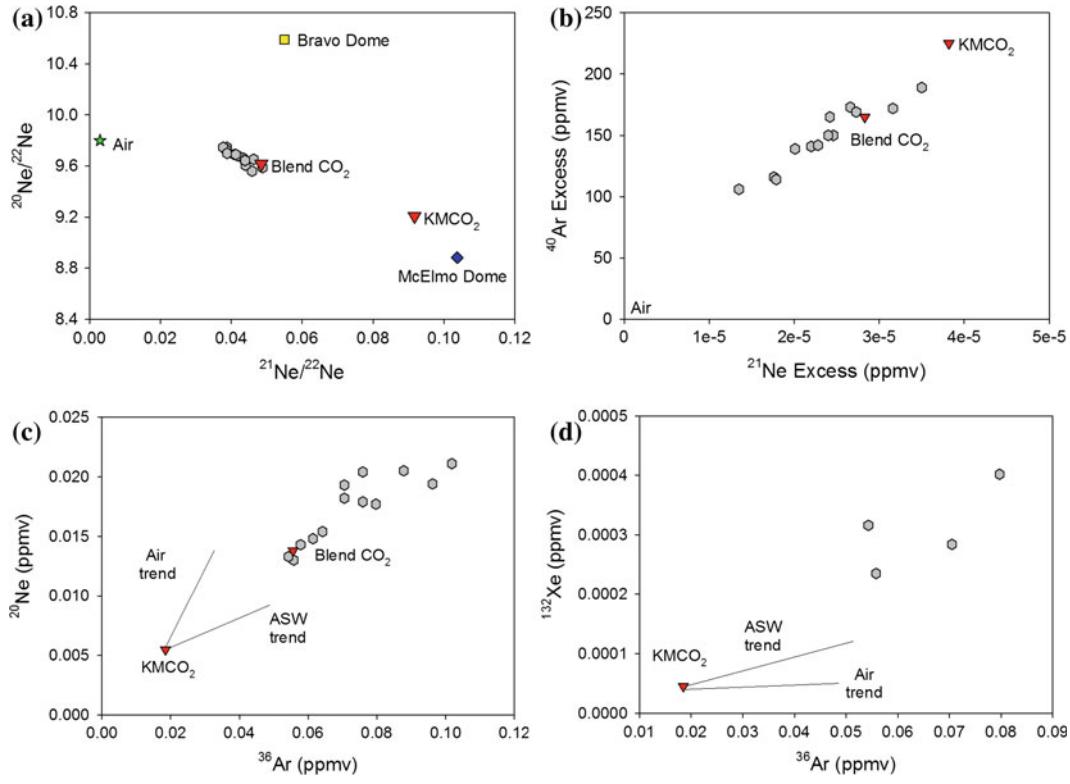

Fig. 17 **a** Plot of $^{20}Ne/^{22}Ne$ against $^{21}Ne/^{22}Ne$ for the individual Mabee oil field samples (*in grey*), $KMCO_2$, which is the composition measured from the incoming CO_2 supply pipeline prior to injection and Blend CO_2 which is from the return pipeline and contains a mix of gases from all the active wells the incoming supply pipeline CO_2. Also plotted is the average Bravo Dome and McElmo Dome ratios from Gilfillan et al. 2008. It is clear to see that the $KMCO_2$ did not originate from Bravo Dome as the operators of Mabee had believed. **b** Plot of the excess ^{40}Ar against excess ^{21}Ne compared to the concentration of air for the Mabee samples including the incoming pipeline CO_2 ($KMCO_2$) and the Blend CO_2. This shows clear mixing between the excess radiogenic ^{21}Ne and ^{40}Ar from the injected $KMCO_2$ and atmospheric air. However the trend does not intersect the origin indicating that an additional crustal component, enriched in ^{40}Ar over ^{21}Ne, must be present. **c** ^{20}Ne concentration plotted against ^{36}Ar concentration. This illustrates that the atmospheric air component in the Mabee samples did not originate from contamination during sampling as the samples do not plot near the fractionation trend expected if the injected $KMCO_2$ was in contact with atmospheric air. They plot on a similar trajectory to what would be expected if the samples were mixing with ASW but with elevated initial ^{20}Ne and ^{36}Ar concentrations. **c** ^{20}Ne concentration plotted against ^{36}Ar concentration. This illustrates that the atmospheric air component in the Mabee samples did not originate from contamination during sampling as the samples do not plot near the fractionation trend expected if the injected $KMCO_2$ was in contact with atmospheric air. They plot on a similar trajectory to what would be expected if the samples were mixing with ASW but with elevated initial ^{20}Ne and ^{36}Ar concentrations. **d** Plot of ^{132}Xe concentration plotted against ^{36}Ar concentration. This plot shows ^{132}Xe concentrations in the Mabee samples are enhanced relative to both the ASW and air fractionation trends starting from an initial $KMCO_2$ composition

injected WAG water in the oil field and hence it is unclear if the crustal radiogenic component was present in this water. However, it is clear from the results of the study that if the groundwaters are the source of crustal radiogenic noble gases, they must have been isolated from atmospheric input for a significant period of time. It is believed that the radiogenic component may originate from the oil reservoir itself as the noble gas compositions measured in the samples from the oil field can be explained by a simple two-component mixture of $KMCO_2$ and a native subsurface component

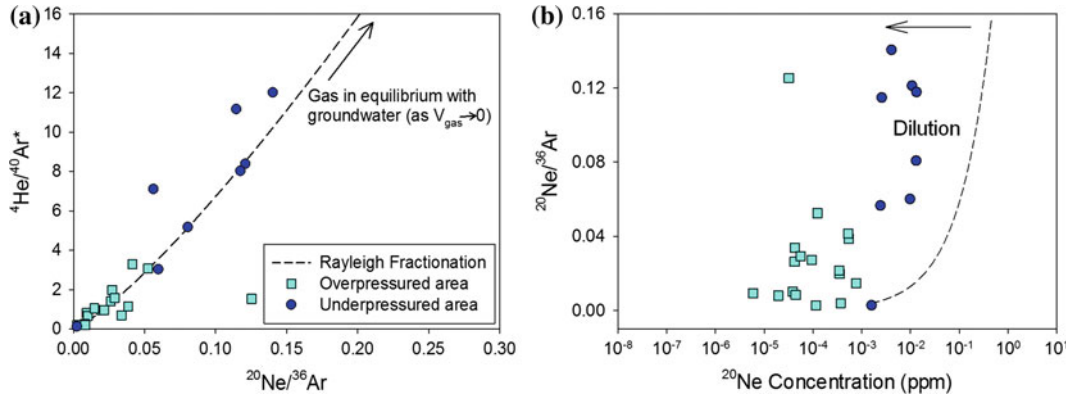

Fig. 18 **a** Water-derived and crustal-derived noble gas show evidence of coherent fractionation trend, which can be modelled as Rayleigh fractionation of a gas phase progressively exsolving from ASW water with a radiogenic component (recalculated and replotted from Zhou et al. 2005). **b** Ne concentrations predicted from the Rayleigh fractionation model are significantly higher than observed, requiring dilution of the groundwater-derived noble gases

which had air-like neon isotope ratios along with a slightly enhanced ^{20}Ne concentration relative to ^{36}Ar, excess ^{40}Ar and enhanced $^{132-136}Xe$ relative to ^{130}Xe.

The key conclusions from this study were: (a) the noble gas tracer was not overprinted in the oil reservoir because the noble gas composition of all of the production gas samples can only be explained by the presence of the $KMCO_2$ component. This is despite the presence of a crustal radiogenic component and a possible WAG component, showing that even if the injected CO_2 moved significantly from the active injection area, the $KMCO_2$ component would still be identifiable, proving that noble gases can be used as tracers of CO_2 migration in a deep reservoir; (b) the sampled $KMCO_2$ had a ^{132}Xe concentration of 1.62×10^{-7} ppmv, which is two orders of magnitude above what would be required for groundsurface monitoring indicating that ^{132}Xe could be used as a tracer of injected CO_2 within the subsurface and probably as a tracer of the migration of deep CO_2.

The noble gas compositions observed in the Mabee Field were very systematic and formed linear trends with only small deviations that could be accounted for by the presence of other known subsurface components, such as a crustal component. This coherent and systematic behaviour of the noble gas system bodes well for using noble gases as tracers of CO_2 in the subsurface. The systematic results obtained from the Mabee study clearly show that even very small isotope variations can be detected using existing noble gas analysis techniques. The isotope variations that would result from injection of artificial noble gas tracers would be much easier to detect and hence Nimz and Hudson demonstrated that noble gases could be used as reliable and robust tracers of CO_2 migration within an engineered storage site.

6.2 Noble Gas Tracing of Groundwater/Coalbed Methane Interaction, San Juan Basin, USA

Coal beds that are not of economic interest for coal extraction are becoming increasingly important as a possible sink for anthropogenic CO_2 emissions (Klara et al. 2003; Pashin and McIntyre 2003). Groundwater plays an important role in CO_2 sequestration in coalbeds in a similar fashion to the controls it exerts on CO_2 storage in CO_2 reservoirs. Consequently noble gases can be used to develop a model of groundwater interaction with coal beds that can inform on the CO_2 sequestering process.

The San Juan Basin natural gas field, located in northwestern New Mexico and southwestern

Colorado in the USA, is a case-type coalbed methane system which was investigated by Zhou et al. (2005). Data from the San Juan field show $^{20}Ne/^{36}Ar$ ratios significantly lower than air but $^{84}Kr/^{36}Ar$ and $^{130}Xe/^{36}Ar$ mostly higher than air which suggests, like the CO_2 fields in the previous section, an open system Rayleigh fractionation process but one in which gas is continuously exsolved and then lost from the system. This can be modelled and, in the case of San Juan data, displayed as the variation in radiogenic $^{4}He/^{40}Ar$ with atmospheric $^{20}Ne/^{36}Ar$. In contrast to the Bravo Dome data, the data converge at the origin when $V_{gas} \rightarrow \infty$ and noble gases have fully exsolved from the fluid phase (Fig. 18a).

However, noble gas data show us this is not the complete story. Using ASW as an initial fluid composition that plausibly fits the San Juan data allows us to predict the ^{20}Ne concentration at any stage of the degassing process (i.e. at any $^{20}Ne/^{36}Ar$). The observed ^{20}Ne concentrations are orders of magnitude lower than predicted (Fig. 18b), as also observed in the CO_2 gas fields of SW USA. In the Bravo Dome CO_2 system, this was explained by CO_2 injection stripping the noble gases from the groundwater, owing to the higher solubilities of noble gases in CO_2 than in water (i.e. the re-dissolution model). However, large scale CO_2 migration is not present in the San Juan basin and hence another explanation is required. The model suggested by Zhou et al. (2005) is that a CH_4 component devoid of any noble gases, and therefore isolated from any groundwater since formation, has diluted the CH_4 component that does contain noble gases from the Rayleigh fractionation process as shown in Fig. 19 (adapted from Zhou et al. 2005).

Further evidence of phase interaction can be identified using the heavy noble gases. In a plot of $^{20}Ne/^{36}Ar$ v $^{130}Xe/^{36}Ar$ (Fig. 13 in Zhou et al. 2005), San Juan data show significant but variable excesses of Xe above that predicted from Rayleigh fractionation. When these Xe data are corrected for the dilution effect of the CH_4 desorbed from the coal bed (the ratio of $[^{20}Ne]$ observed divided by $[^{20}Ne]$ modelled), the Xe excesses disappear and the model fits the data excellently. This independent evidence of a dilution effect from Xe enriched coal corroborates the model presented in Fig. 19. This in turn shows that groundwater is not the only control on coal biodegradation and therefore groundwater alone does not determine the viability of coal beds as a CO_2 sequestration reservoir: other important factors include overpressure that may help maintain the integrity/isolation of coal bed seams.

As described in the Sect. 5, step-wise equilibrium degassing can approximate Rayleigh fractionation if at each stage of degassing, V_{gas}/V_{water} is small. In this case study, the differences between the modelled and observed Ne concentration can be quantified (Fig. 18b). Using this dilution ratio together with calculations of gas production history as performed on the CO_2 data in Sect. 5 (for details of this case study see Table 3 Zhou et al. 2005) one can quantify the volumes of water associated with a gas producing well. Assuming coal bed thickness and specific porosity, one can calculate the volume of water involved in gas production of specific wells. Expressed as radii from the well, in the San Juan field these volumes vary from 16 to 242 m (Zhou et al. 2005). This is significantly smaller than the distance between wells. This in turn indicates there is no need for dynamic groundwater flow between wells on the timescale of well gas production and, in this case, suggest that more CH_4 wells can be drilled without adversely affecting existing well gas production.

In the context of the carbon sequestration, this information is important for understanding reservoir connectivity and the presence of absence of continuous water flow through a basin in light of the evidence that the majority of CO_2 sequestration analogues contain CO_2 dissolved in groundwater (see Sect. 5). In

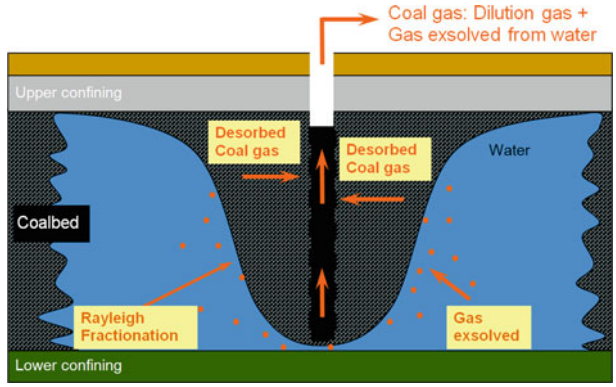

Fig. 19 Cartoon of Rayleigh fraction and dilution model adapted from Zhou et al. 2005. Gas exsolved from the ASW is heavily fractionated and diluted with gas desorbed from the coal bed that has not previously interacted with the groundwater system and is therefore devoid of noble gases

exhausted CO_2 reservoirs or basins undergoing enhanced oil recovery, this type of analysis may also provide information on the extent to which new drilling may increase the storage capacity of a potential subsurface CO_2 storage site.

7 Use of Noble Gases for Monitoring of Subsurface CO_2 Migration and Leakage

7.1 Noble Gases as Tracers of CO_2 Leakage at Green River Springs, Utah, USA

Wilkinson et al. (2010) examined naturally occurring noble gas tracers and isotopic ratios from surface gas samples from a suite of natural CO_2 springs. These springs provide an analogue for some time in the future, when a very severe failure of a containment site has been detected after injection operations have ceased. In the imagined scenario, there was a reservoir of artificially injected CO_2 which existed as a discrete fluid together with shallower aquifers which also contain natural CO_2. It was imagined that a baseline survey had not been undertaken prior to CO_2 storage commencing, so there was only proxy information available from regional archives to identify the chemistry and gas contents of the diverse shallower CO_2 sources and aquifers. The key questions that the study aimed to address were; could CO_2 migration from an injection zone, through the overburden, to the surface, be quantified? Could different sources of CO_2 be discriminated?

The group of CO_2-rich springs sampled by Wilkinson et al. (2010) were located 10 km south of the town of Green River, southwest Utah. They are CO_2-charged springs associated with the Little Grand Wash and Salt Wash faults lying at the northern end of the Paradox Basin in south west Utah. These control the present day flow of gas and groundwater to the surface (Heath 2004; Shipton et al. 2004) with both being part of a series of steeply dipping (70–80°) WNW trending normal faults that are found in the region. Springs of CO_2-rich water and free gas, an active CO_2 charged geyser, and both active and fossil travertine deposits are associated with the Little Grand Wash fault zone. The most notable spring is the cold-water CO_2-charged Crystal Geyser, which erupts to heights of up to 25 m at 4–12 h intervals (see Shipton et al. 2004 for further details). In addition to Crystal Geyser, numerous CO_2-charged springs are associated with the Salt Wash fault zone (see Heath (2004) for further details).

The gases emitted by the Green River Springs are predominantly CO_2 but also include nitrogen and trace noble gases (Heath 2004). Prior to the study of Wilkinson et al. CO_2 and other gases in

the springs were considered to originate from a combination of sources including mantle-degassing, clay-carbonate reactions, the thermal metamorphism of carbonates or atmospheric and soil gas recharge combined with diagenetic reactions such as the maturation of organic material.

In order to calculate crustal and mantle inputs to the CO_2, Wilkinson et al. first quantified the amount of air present in each sample. This was calculated using the measured $^{40}Ar/^{36}Ar$ ratio for each spring using the following formula:

$$\left[^{40}Ar\right]_{air} = \left[^{40}Ar\right]_{meas} \times \left(^{40}Ar/^{36}Ar\right)_{air} / \left(^{40}Ar/^{36}Ar\right)_{meas} \quad (19)$$

The proportion of air-derived Ar was found to be high (33–91 %) as a result of the high ^{40}Ar content of the atmosphere, compared to the much lower crust and mantle contributions. Figure 20 clearly shows how the amount of dissolved air in the samples was controlling both the $^{40}Ar/^{36}Ar$ and $^{4}He/^{20}Ne$ ratios. Using the air-derived ^{40}Ar concentration, it was straightforward to calculate the air contribution to the total erupted CO_2 using the known $CO_2/^{40}Ar$ for air of 0.0398 (Porcelli et al. 2002). The air contribution to the CO_2 was found to be insignificant (0.00003 to 0.00018 volume % CO_2).

The measured $^{3}He/^{4}He$ of the gases erupting from the springs showed a small variation from 0.224 to 0.265 R_a, with the exception of Pseudotenmile geyser which exhibited a higher ratio of 0.386 R_a. This spring was also noted to have a very slow gas discharge rate, possibly enabling atmospheric noble gases to become dissolved in the spring water to form a component of the measured gas, possibly explaining the higher $^{3}He/^{4}He$ ratio observed.

Using the established technique (Craig et al. 1978) the authors attempted to correct the measured $^{3}He/^{4}He$ ratios for the air component, leaving just the crust and mantle input. However, the correction was very small and significantly less than the precision of the data. This was unsurprising given the measured range of $^{4}He/^{20}Ne$ of 313 to 13,002, significantly above the air value of 0.288 (Ballentine et al. 2002). All of the $^{3}He/^{4}He$ ratios were significantly higher than the crustal $^{3}He/^{4}He$ ratio of 0.02 R_a but also lower than the sub-continental mantle ratio of 6 R_a (Fitton et al. 1991). Using these end-member values, it was possible to calculate the proportion of the He from both crustal and mantle sources using the following formula (from Ballentine et al. (2002)).

$$^{4}He_{crust} = \left(^{4}He_{measured} \times {}^{3}He/^{4}He_{mantle} - {}^{3}He/^{4}He_{measured}\right) / \left(^{3}He/^{4}He_{mantle} - {}^{3}He/^{4}He_{crust}\right) \quad (20)$$

The crustal contribution to ^{4}He in the samples ranged from 94 to 97 % with the remainder originating from the mantle. It was also possible to calculate the crustal contribution to the measured ^{3}He concentration using the known continental crust $^{3}He/^{4}He$ ratio of 0.02 R_a. Only 5–8 % of the total ^{3}He originated from the crust with the remainder from the mantle.

The known range of mantle $CO_2/^{3}He$ ratios was used (1×10^{9} to 1×10^{10}) to calculate the proportion of CO_2 which had originated from both the mantle and crust, knowing the atmosphere contribution to the CO_2 was negligible. An unknown is the crustal $CO_2/^{3}He$ ratio, which is variable (O'Nions and Oxburgh 1988). However, a simple mass balance approach allowed the crustal $CO_2/^{3}He$ ratio to be calculated.

$$^{3}He_{mantle} \times CO_2/^{3}He_{mantle} + {}^{3}He_{crust} \times CO_2/^{3}He_{crust} = 1 \quad (21)$$

The results of these calculations are shown in Table 4. Using a $CO_2/^{3}He$ ratio of 1×10^{9} the crustal contribution of CO_2 is uniformly between 84 and 99 % of the total CO_2. Use of a $CO_2/^{3}He$ ratio of 1×10^{10} gives a wider range of crustal compositions ranging from 0 % for Tenmile Geyser to 98 % for Big Bubbling Spring. Unfortunately from these results, it is not possible to determine if the crustal component was derived from deep crustal reactions, or from aquifer water that had interacted with crustal minerals. The calculated $CO_2/^{3}He$ ratios for the crust ranged from 5.81×10^{10} to 6.53×10^{12},

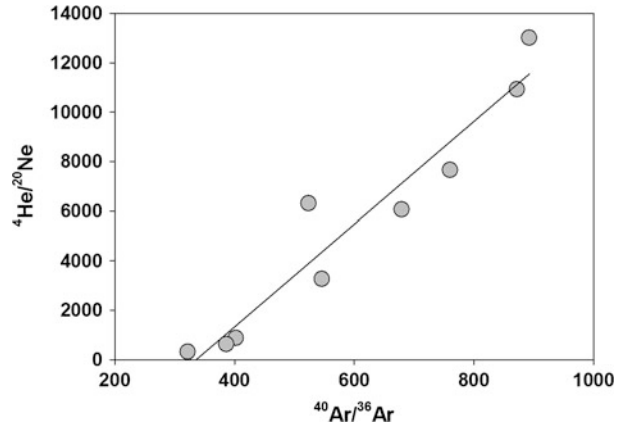

Fig. 20 Plot of $^{4}He/^{20}Ne$ against $^{40}Ar/^{36}Ar$ for the Green River Springs. It is clear that the quantity of dissolved air in the samples is controlling both the $^{40}Ar/^{36}Ar$ and $^{4}He/^{20}Ne$ ratios, with the greatest amount of air in the samples with the lowest ratios

Table 4 Calculated origins of CO_2 erupted at Green River Springs

Sample	Using $CO_2/^3He$ of 1×10^9			Using $CO_2/^3He$ of 1×10^{10}		
	CO_2 origin %		Crust $CO_2/^3He$			Crust $CO_2/^3He$
	Crust	Mantle		Crust	Mantle	
Tumbleweed	98.7	1.3	7.82×10^{11}	86.7	13.3	6.87×10^{11}
Torrey's Spring	96.9	3.1	3.33×10^{11}	68.8	31.2	2.37×10^{11}
Main vent—Crystal Geyser	99.7	0.3	4.88×10^{12}	97.4	2.6	4.77×10^{12}
Side seep—Crystal Geyser	99.5	0.5	2.34×10^{12}	94.6	5.4	2.22×10^{12}
Chaffin Ranch	96.9	3.1	3.45×10^{11}	69.1	30.9	2.46×10^{11}
Small Bubbling Spring	99.6	0.4	3.26×10^{12}	96.2	3.8	3.15×10^{12}
Big Bubbling Spring	99.8	0.20	5.64×10^{12}	98.0	2.0	5.53×10^{12}
Pseudotenmile Geyser	99.7	0.30	6.53×10^{12}	97.0	3.0	6.35×10^{12}
Tenmile Geyser	84.4	15.6	5.81×10^{10}	0	100	–

which are within the range considered by O'Nions and Oxburgh (1988) to be typical of the crust.

In this study noble gas tracers provided substantial constraints on the origins of CO_2 erupted at the Green River Springs, and hence were much more useful than stable isotope data alone. However, due to the lack of measured baseline data on the noble gas composition and CO_2 contents of the different aquifers beneath the springs, noble gases could not provide an unequivocal determination of the origin and transport mechanisms of the CO_2 erupted (Fig. 21).

It was possible to determine that the erupted CO_2 is largely derived from crustal sources, with a 0.2–31 % contribution from the mantle, with the exception of a single spring (Tenmile Geyser) that could be erupting mostly mantle CO_2. This origin for the erupted CO_2 is in contrast to the large, commercially exploited CO_2 accumulations that surround the Colorado Plateau, which are of purely mantle origin. Hence, Wilkinson et al. (2010) were able to determine that the Green River Springs are not derived from these large accumulations. Additionally, they also found that the Green River Springs' noble gases are quite variable in composition,

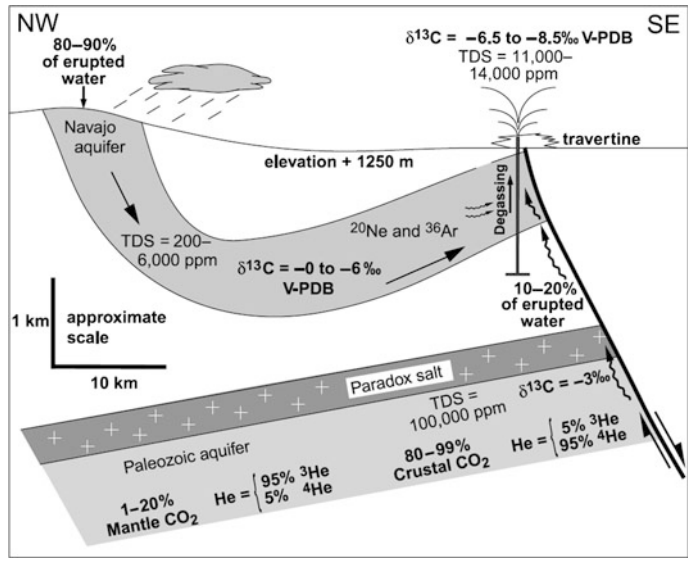

Fig. 21 Cartoon summary of the imagined CO_2 sources beneath the Green River Springs. There is no evidence in the noble gas data for a large subsurface accumulation of free CO_2 (Wilkinson et al. 2010)

arguing against a homogeneous reservoir of free phase CO_2 within the shallow Navajo Aquifer. Nevertheless, they also argue that some ascent of free CO_2 gas must have occurred because the measured surface volumes contained too much CO_2 to have been dissolved in the volume of water erupted at the springs. It is clear from this study that the CO_2 is not derived from a single reaction or source, as had been previously assumed, but is predominantly from crustal diagenetic reactions within the shallow Navajo Aquifer, except for the 1–31 % mantle contribution thought to have originated from the much deeper Paleozoic aquifer.

Whilst the noble gas tracers were not entirely diagnostic of the processes forming the CO_2, with uncertainty still surrounding CO_2 origin and transport mechanisms, the detection of leaks in engineered storage scenarios should be easier as the CO_2 will have a distinctive isotopic composition. Additionally a comprehensive baseline survey will be required at any proposed storage site and with better baseline geochemical data, more would be possible.

7.2 He and Rn in Soil Gases and CO_2 Seeps from the Massif Central, France

An extensive geochemical study of natural CO_2 release at the surface was undertaken by Battani et al. (2010) in Sainte-Marguerite, in the Massif Central region of France. This examined soil gas fluxes and concentrations as well as gas from CO_2 rich bubbling springs. These seeps provide a natural laboratory to study CO_2/fluid/rock interactions and the migration mechanisms of CO_2 migration to the surface. The Sainte-Margurite region is located in the southern part of the Limagne graben and contains many CO_2-rich springs caused extensive natural emissions of CO_2. The springs sampled were associated with two major fault systems dating from the tardi-Hercyian period. The area also contains travertine deposits associated with the CO_2-rich springs.

Soil gas measurements were made over a small area (50 × 100 m) surrounding an ancient thermal bath over two field campaigns in 2006

and 2007. ^{4}He and ^{222}Rn abundance measurements of the soil gases were made in the field and gas samples were also collected for analysis in the laboratory for noble gas abundances, isotopes and $\delta^{13}C$ (CO_2) isotopes. All samples for laboratory analysis were collected using a micro gas chromatograph as a pump to collect gases from depth of 1 m. N_2, Ar and O_2 peaks were monitored during collection to ensure atmospheric gases had been purged from the collection system. Samples of gas were also collected from numerous CO_2 rich bubbling water springs, inferred to be deep gas (Battani et al. 2010).

Measured helium isotopic ratios in the CO_2 exsolving from the bubbling springs ranged from 0.76 to 6.62 R_a. The upper value indicates some samples contain a pure mantle component, given it is above the European Sub Continental Lithopsheric Mantle (SCLM) value of 6 R_a (Gautheron and Moreira 2002) and close to the upper mantle value of 8 R_a (Kurz and Jenkins 1981). Additional evidence of a predominantly mantle origin for the CO_2 came from the measured $\delta^{13}C$ (CO_2) values which were close to −5 %, within the range of mantle derived CO_2 (Marty and Zimmermann 1999). Measured ^{4}He concentrations ranged from 0.12 to 39.12 ppm and somewhat surprisingly the majority of the samples exhibited lower ^{4}He concentrations than the atmospheric value of 5.24 ppm. The low ^{4}He concentrations were particularly unexpected given that the springs emerge from granitic basement which is typically rich in U and Th and hence, as a result of their radioactive decay, also ^{4}He. Battani et al. (2010) argue that this result can only be explained if the fluids migrate rapidly from depth to the atmosphere, and do not interact with crustal fluids. The rapid migration of the CO_2 gas is further confirmed by the observed Ar isotopic fractionation, which is consistent with a Rayleigh type fractionation process. This is illustrated in Fig. 22, which shows that both Ar isotopic ratios ($^{38}Ar/^{36}Ar$ and $^{40}Ar/^{36}Ar$) follow the Mass Fractionation Line (MLF). Such mass fractionated values are a strong indication of a fast migration process which does not allow time for re-equilibration with other fluids. The gas was therefore assumed to travel fast along the deep-rooted faults of the granitic basement.

This is a significantly different scenario to that observed at the Green River Springs in the Colorado Plateau (Sect. 7.1), where the noble gas and $\delta^{13}C$ (CO_2) data indicated that most of the CO_2 was dissolved in water at depth prior to degassing at the surface.

The $\delta^{13}C$ (CO_2) of the soil gas samples ranged between −3 and −5.1 %, slighter heavier than those measured in the CO_2 degassing from the Bubbling Springs, indicating either a crustal or mantle origin of the gas. Battani et al. argued that this was the result of interaction of the gas with the local travertines, which have a $\delta^{13}C$ signature of between 4.4 and 7.4 % (Casanova et al. 1999). Thermal breakdown of travertine would also explain the higher than mantle $CO_2/^{3}He$ ratios which were measured in the gases from some of the bubbling springs. This interaction between soil gas and travertine was consistent with the measured ^{222}Rn activity, as the soil gas samples from above the travertine deposits exhibited higher activities, reaching up to 2×10^{6} Bq/m^{3}. Travertines are between 300 to 10,000 times more enriched in uranium and thorium than typical surface sediments (Casanova et al. 1999). Comparing the soil gases that contained over 50 % by volume of CO_2 with radon activities in excess of 50,000 Bq/m^{3} indicated a strong correlation between the two gases. The enriched Rn activity allowed the authors to identify preferential pathways for migration of gas from depth in the soil gas samples which trended NE-SW aligned to the Allier-river axis, a structure of related to the former opening of the Limagne graben.

The soil gas He concentrations were less diagnostic as both low (less than 5 ppm) or high (over 6 ppm) helium values were exhibited by the samples with high measured high CO_2 concentrations. However, significantly lower than atmosphere values of Ar were measured and this was attributed to the soil gases containing a significant amount of the deep gas flux also found in the bubbling springs. Despite the lack of a clear correlation of high CO_2

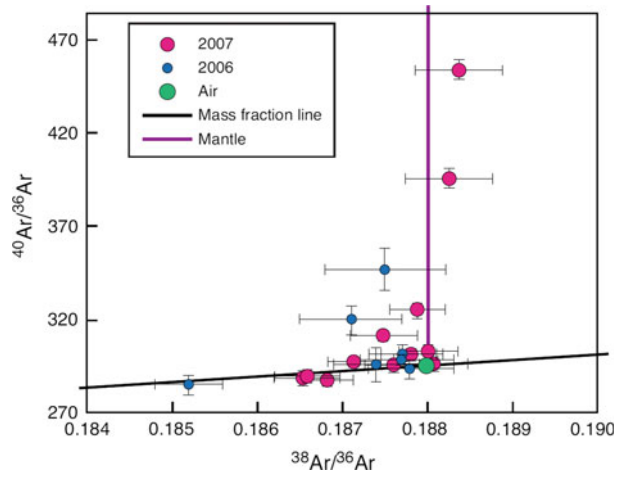

Fig. 22 Plot of $^{40}Ar/^{36}Ar$ against $^{38}Ar/^{36}Ar$ from the CO_2 exsolving from the bubbling springs. This illustrates that the majority of the samples plot along the *black* mass fractionation *black line*. Battani et al. (2010) argued that the increase of some $^{40}Ar/^{36}Ar$ ratios could either be explained by a mantle derived input or the addition of a small component of radiogenic $^{40}Ar^*$. This type of kinetic fractionation is indicative of rapid migration of the fluid

concentrations with He, this study highlighted the role that multiple noble gases (in this case He, Ar and Rn) and C isotopes can play in identifying the migration of CO_2 from depth. It also reinforced the importance of a detailed background geochemical study prior to a storage site being utilised, in order to determine the natural noble gas and C isotope geochemistry which might not be as predicted (i.e lack of ^4He in the deep CO_2 and high natural $^3He/^4He$ as observed in this work).

7.3 He and Ne as Tracers of Natural CO_2 Migration at St. Johns Dome, Arizona, USA

An important aspect of engineered CO_2 storage is the ability to monitor the storage site, and to trace the CO_2 after injection. Future engineered CO_2 storage sites will consist of both the reservoir or saline formation into which the CO_2 is injected, and the overlying suite of rocks above the reservoir or saline formation up to the ground surface. Hence, the overburden will become legally defined as part of the 'storage complex' (EU 2009), and its containment performance needs to be evaluated to ensure that CO_2 can be safely stored over geological timescales. However, it is extremely difficult to unequivocally detect the small releases of anthropogenic CO_2 that could arise from a diffuse leakage of CO_2 from a storage site. This is because there are many natural sources of CO_2 within the crust with overlapping signatures, including breakdown of carbonate minerals or cements, biological activity or hydrocarbon oxidation. Therefore, a more specific and unambiguous method is needed to fingerprint deep-derived CO_2 migration, but it has not yet been understood if fingerprints remain intact during hundreds of metres of migration and diverse interacting geochemical and petrophysical processes.

As an analogue for post-emplacement seepage, Gilfillan et al. (2011) have recently examined natural CO_2 rich springs and groundwater wells in the vicinity of the St. Johns Dome CO_2 reservoir located on the border of Mid-Arizona/New Mexico, USA. Extensive travertine deposits surrounding the CO_2 reservoir highlight a past history of migration of CO_2 rich fluids to the surface. However, there is no evidence that travertine formation is occurring at present and no geysers with gaseous CO_2 are currently found

in the area (Moore et al. 2005). High concentrations of HCO_3^- are common in surface springs, shallow groundwater wells used for irrigation and deeper wells used to obtain cooling water for a coal fired power plant in the region. Previous chemical analysis of these waters implied a possible connection between the formation water within the CO_2 reservoir and the HCO_3^- rich water. This link was not found to be conclusive, due to significant differences in water types (Moore et al. 2005) and the fact that a soil gas survey surrounding these springs and wells was unable to differentiate additional CO_2 flux from that of background biological activity (Allis et al. 2005).

$\delta^{13}C$ measurements have proven to be extremely valuable in tracing CO_2 injected into early CO_2 storage test sites, such as Weyburn (Raistrick et al. 2006). However, in the St. Johns Dome waters there was no clear relationship between the HCO_3^- content of and the $\delta^{13}C_{DIC}$ ratio or sample depth (Fig. 23a). This was in stark contrast to the relationship observed between HCO_3^- concentration and $^3He/^4He$, which showed a distinction between the above air ratios measured in three spring water samples (Willowbank Spring, 24 Bar Ranch and New Mexico Spring—hereafter termed the anomalous springs) and the below air $^3He/^4He$ measured in all of the other samples (Fig. 20b). The above air values in the three springs were attributed to the presence of a small amount of excess ^3He produced by tritium decay, indicating a contribution of recent tritium bearing water. There was also a marked distinction in both the ^3He and ^4He concentrations measured in these three anomalous samples, which were an order of magnitude lower than other water samples (Fig. 23). With the exception of Colorado River Spring, all of the remaining water samples exhibited higher HCO_3^- concentrations which corresponded to lower $^3He/^4He$ ratios (Fig. 23b).

Significantly higher than atmosphere concentrations of ^4He in all of the groundwater wells and majority of surface springs implies the addition of a crustal component that had accumulated radiogenic ^4He. Thus, a portion of the water originated at depth, having circulated in the crust for a significant period of time (Torgersen and Clarke 1985). The ^4He excess was further illustrated by the significantly above air $^4He/^{20}Ne$ measured in all water samples, excluding the similar to air values measured from the three anomalous springs. Figure 24a shows that the low $^3He/^4He$ and high ^4He within the groundwater wells and majority of surface springs (bar the three anomalous springs) could be explained by simple mixing between low $^3He/^4He$ and high ^4He values measured in Wells 10–22 and 22–1X and varying percentages of shallow groundwater (high $^3He/^4He$ with low ^4He concentrations). This clearly illustrated that the excess ^4He fingerprint entrained at depth was retained after migration of the waters to the surface.

As with ^4He, the low $^3He/^4He$ and corresponding high ^3He values within the deep groundwater wells and most surface springs, could be explained by simple mixing between water from Wells 10–22 and 22–1X and air (Fig. 24b). This clearly indicated that all of the waters rich in ^3He must have interacted to some degree with the magmatic CO_2 in the deep reservoir. Furthermore, the fingerprint of high ^3He from magmatic origin, exhibited by the deep CO_2 wells, although diluted, was also retained during transport of water and CO_2 to the surface.

All of the sampled waters, bar the three anomalous air-like springs, exhibited $CO_2/^3He$ ratios which were extremely similar to the range observed in the three deep CO_2 wells (Fig. 25a and b). These results further reinforce the observation that all of the water samples, except for the anomalous springs, contained CO_2 of magmatic origin, which had originated from the CO_2 reservoir. The higher $CO_2/^3He$ ratios observed in the three anomalous springs indicated that they contained CO_2 with less ^3He content compared to that of the deep reservoir, providing further evidence that the anomalous springs contain additional CO_2 from a different source. Several samples exhibited ratios below the lowest observed CO_2 well value of 9.75×10^7, which implied that some of the CO_2 component had been lost relative to ^3He.

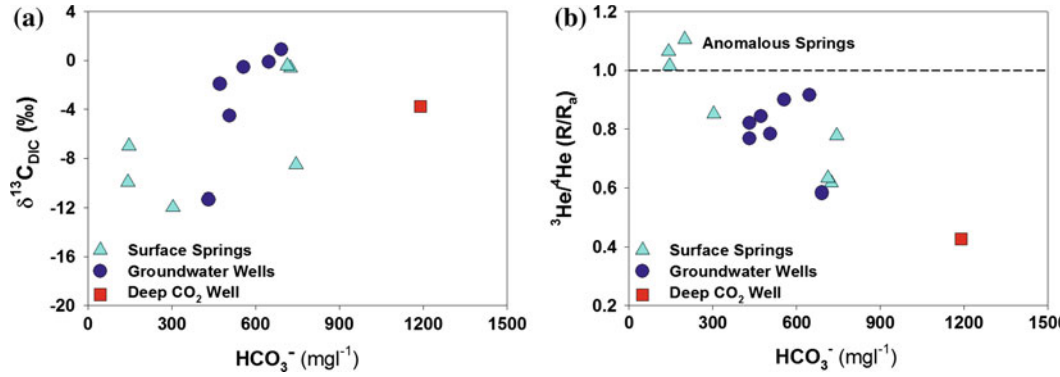

Fig. 23 **a** $\delta^{13}C_{DIC}$ variation plotted against HCO_3^- concentrations for the surface springs, groundwater and CO_2 well sampled at St. Johns. There is no clear relationship between the HCO_3^- concentration of the water and $\delta^{13}C$ or the sample type. **b** $^3He/^4He$ ratios plotted against HCO_3^- concentrations for the surface springs, groundwater and CO_2 well sampled at St. Johns. Values obtained from groundwater wells cluster above $^3He/^4He = 1$, equating to air. A clear correlation exists between increasing HCO_3^- concentrations and decreasing $^3He/^4He$, trending toward the values measured in the deep CO_2 reservoir. A clear distinction existed between the above air $^3He/^4He$ ratios measured in three anomalous spring water samples; Willowbank Spring, 24 Bar Ranch and New Mexico Spring and the other water samples

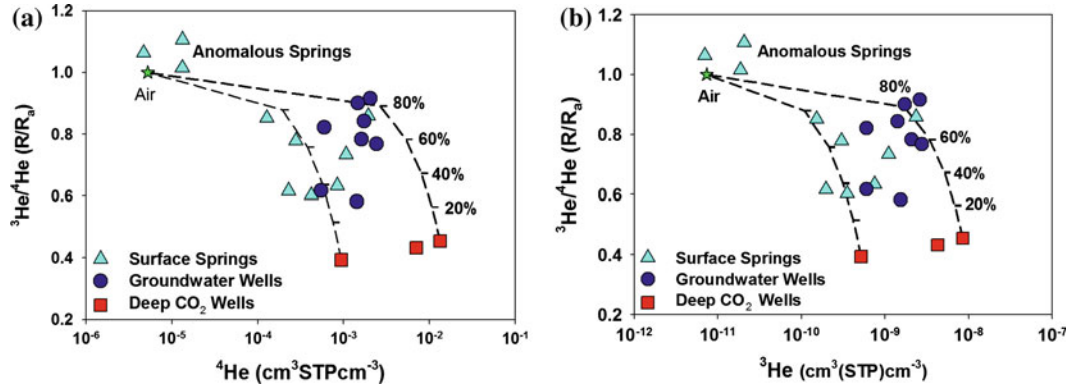

Fig. 24 **a** ^4He plotted against $^3He/^4He$ for the St. Johns waters. *Mixing lines* are plotted from the different compositions of deep groundwater measured from the end member CO_2 wells to 100 % air. The low $^3He/^4He$ and high ^4He within the groundwater wells and majority of surface springs can be explained by simple mixing between the $^3He/^4He$ and ^4He values measured in Wells 10–22 and 22–1X and varying amounts of air (with the per cent air indicated on *tick marks*). This proved that the excess ^4He component entrained at depth was retained and not lost on migration of the waters to the surface. **b** ^3He plotted against $^3He/^4He$ for the St. Johns water samples. As with ^4He, high ^3He concentrations and low $^3He/^4He$ ratios were observed in groundwater wells and majority of the surface springs. These can also be accounted for by the mixing of waters from wells 10–22 and 22–1X and varying amounts of air. This shows that the whilst the high magmatic ^3He signature exhibited by the deep CO_2 wells, although diluted, was retained and not lost as a result of transport water to the surface

Gilfillan et al. (2011) also documented a clear relationship between $CO_2/^3He$ reduction and increases in both ^{20}Ne and especially ^4He (Fig. 25) within the St. Johns water samples. As previously outlined in this chapter, similar relationships have been observed in numerous CO_2 reservoirs around the world (Gilfillan et al. 2009; Sherwood Lollar and Ballentine 2009). Whilst there are means by which crustal CO_2 ($CO_2/^3He > 10^{10}$) could be added to an initial

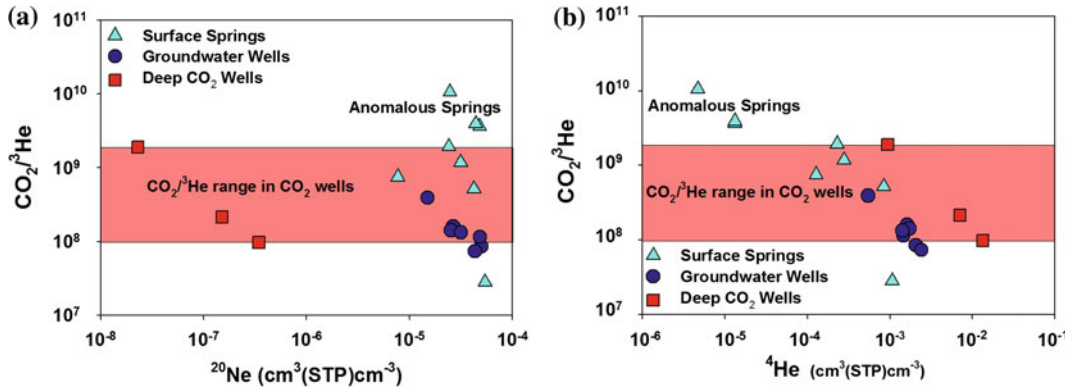

Fig. 25 **a** $CO_2/^3He$ variation plotted against ^{20}Ne for the St. Johns water samples. All of the groundwater springs and the majority of the surface springs exhibit $CO_2/^3He$ ratios which are extremely similar to those measured in the deep CO_2 wells, so implying that they contain dissolved CO_2 which migrated from the CO_2 reservoir. A clear trend of decreasing $CO_2/^3He$ with increasing ^{20}Ne existed in all of the data. As ^3He is a conservative tracer, reduction of $CO_2/^3He$ can only be explained by a reduction of the CO_2 component. As the groundwater is the main source of ^{20}Ne, this CO_2 reduction must be linked to contact with the groundwater. **b** $CO_2/^3He$ variation plotted against ^4He for the St. Johns samples. A clear reduction in the $CO_2/^3He$ ratio corresponds to an increase in ^4He. This can be explained by the mixing of ^4He, which has accumulated in the deep formation water, with the younger shallow groundwater and then migrating from the reservoir, along with dissolved CO_2. This trend is identical to that observed in natural CO_2 reservoirs from around the world (see Fig. 9)

mantle rich CO_2 accumulation (Bradshaw et al. 2004; Cathles and Schoell 2007), there is no plausible mechanism that would allow crustal CO_2 to be added whilst preserving the correlation between $CO_2/^3He$ reduction and increases in noble gases derived from the groundwater. Hence, the changes in $CO_2/^3He$ must be due to CO_2 loss in the subsurface by an amount directly related to the quantity of groundwater that the CO_2 has contacted. As CO_2 is soluble and reactive, the most probable mechanisms of subsurface CO_2 fluid phase removal are dissolution of the CO_2 into the groundwater and/or mineral trapping (Baines and Worden 2004b; Bradshaw et al. 2004). As previously highlighted earlier in this chapter it has been possible in some natural CO_2 reservoirs to distinguish between proportions of CO_2 that were dissolving into the formation water and those which were precipitating as carbonate minerals (Gilfillan et al. 2009). However, due to the lack of any correlation between the $\delta^{13}C$ and $CO_2/^3He$ this was not possible within the St Johns water samples.

The results of this study illustrate that the He and Ne concentrations and $^3He/^4He$ and $CO_2/^3He$ ratios provide characteristic fingerprints, which could be identified in all of the groundwater wells and all but three of the surface springs. The simplest explanation is that the groundwater wells sampled shallow well and spring waters containing noble gases together with magmatic CO_2 derived from the deep reservoir. In this model, the high concentrations of HCO_3^- present in the sampled waters are then the direct result of the migration of dissolved CO_2 from the deep reservoir, illustrating for the first time that CO_2 can be fingerprinted from source to surface using noble gases, particularly He. This paves the way for the use of similar techniques to identify dissolved CO_2 migration from future engineered storage sites.

7.4 Noble Gas Investigation of Alleged CO_2 Leakage at Weyburn

In January 2011 it was extensively reported that the Kerr family had been forced to move from their property located above the Weyburn-Midale Monitoring and Storage Project in Saskatchewan,

Canada. A geochemical consultant from Petro-Find GeoChem Ltd., who was hired on behalf of the Kerr's, reported measurements of $\delta^{13}C$ (CO_2) isotope values in soil gases rich in CO_2 which were similar to those of the CO_2 injected into the deep oil reservoir (Lafleur 2010). The Petroleum Technology Research Centre (PTRC), who are responsible for the environmental monitoring of the Weyburn CO_2-EOR and storage operation, published a detailed response correctly stating that Petrofind had not taken the similar baseline $\delta^{13}C$ (CO_2) isotope measurements conducted prior to the injection into account (Petroleum Technology Research Centre 2011). Also as $\delta^{13}C$ (CO_2) is not a unique tracer, there were several other natural sources that could account for the measured values. Whilst this response went some way to addressing the public perception fears raised by the alleged CO_2 leakage claims, it was clear that more research was required to re-establish confidence in the safety and security of CO_2 stored at Weyburn. This was imperative for both the project itself and the future acceptance of the safety and security of CO_2 storage technologies. The International Performance Centre for Geologic Storage of CO_2 (IPAC-CO_2) undertook a detailed independent incident response protocol focused on the near surface soil gases, the noble gas composition of the shallow groundwaters and a hydrogeological analysis. In the following section we summarise the findings of the noble gas investigation.

In order to determine if migration of dissolved CO_2 from the Weyburn oil field was responsible for the alleged CO_2 anomaly, Gilfillan and Haszeldine (2011) completed noble gas measurements on water samples collected from four groundwater wells surrounding the Kerr quarter, near Goodwater in Saskatchewan. These were compared to the noble gas composition measured from fluids obtained from a production well and CO_2 and water obtained from two separate injection wells on the Weyburn-Midale oil field, located near to the Kerr quarter. The aim of the work was to test the hypothesis that migration of dissolved CO_2, originating from either the free phase CO_2 or water injected into the Weyburn-Midale oil field or from CO_2 contained in the produced fluids, was responsible for the CO_2 anomaly reported at the surface. This focused on dissolved CO_2 in the groundwaters as no free phase CO_2 was present in the sampled well waters and as recent research has shown that the sensitivity of He as a tracer is two orders of magnitude greater in groundwaters than in soil gases (Mackintosh and Ballentine 2012).

Gilfillan and Haszeldine (2011) found that the measured $^4He/^{20}Ne$ ratios in the injected CO_2 and produced fluid samples were significantly above the calculated air saturated water range of 0.250 to 0.296 (Fig. 26). This indicated that atmospheric He input to these samples was minimal. The injected water $^4He/^{20}Ne$ ratio of 1.42 implied that there was a small amount of atmospheric He input in this sample. However, this was considerably above the range of 0.248 to 0.403 observed in the groundwater samples. This overlapped with the air saturated water range (assuming a 0–50 % excess air component and a re-equilibration temperature range on 10 to 25 °C) and indicated that almost the entire of the ^4He dissolved in the groundwaters was of atmospheric origin.

Similarly, there was a distinct difference in $^3He/^4He$ ratios in the different sample types, with the lowest values of 0.173 and 0.179 R_a measured in the produced CO_2 from the Weyburn field (Fig. 26). The injected CO_2 had a similar, albeit slightly higher ratio of 0.193 R_a, with the injected water sample ratio being higher again at 0.295 R_a. The range observed in the groundwater samples of 0.897 to 1.103 R_a was significantly above the ratios observed in the produced fluids, injected water and CO_2 samples, consistent with the $^4He/^{20}Ne$ ratios in indicating that almost the entire of the ^4He in the groundwater samples originated from the atmosphere.

^4He and ^{40}Ar concentrations also exhibited marked distinctions depending on sample type (Fig. 27). The lowest ^4He concentrations were those calculated for water equilibrated with the injected CO_2. The groundwater samples exhibited a measured range of ^4He which was similar to the calculated air saturated water concentration range. This clearly showed that there was no

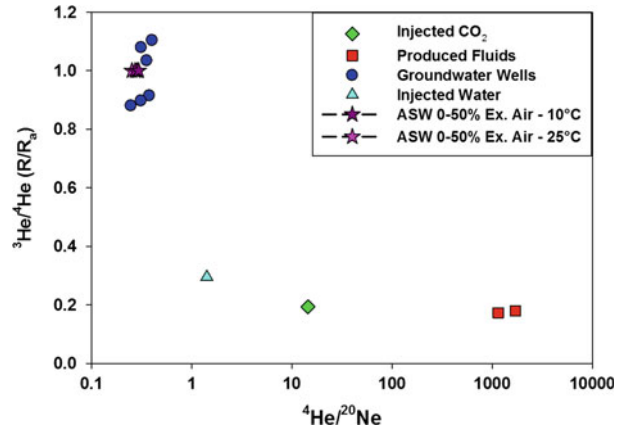

Fig. 26 $^3He/^4He$ ratios plotted against $^4He/^{20}Ne$ ratios. The produced CO_2 and injected CO_2 exhibited ratios well in excess of the air saturated water values. The groundwater wells were extremely close to the air saturated water (ASW) ratio range indicating that almost all of the ^4He they contain is of atmospheric origin (Gilfillan and Haszeldine 2011)

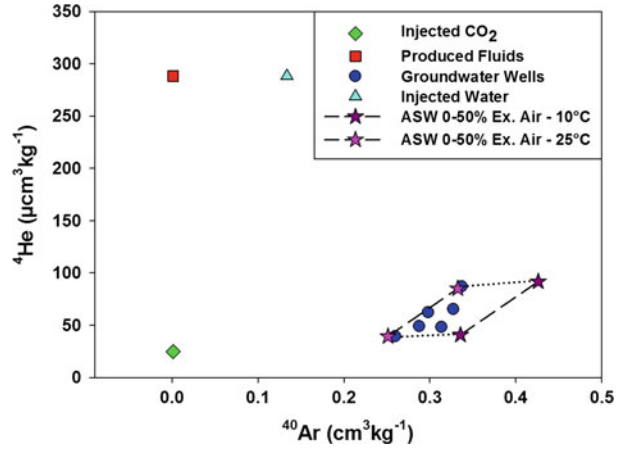

Fig. 27 ^4He concentration plotted against ^{40}Ar concentration. All of the groundwater samples plot within the air saturated water (ASW) concentrations indicating that there is no input of crustal ^4He and the ^{40}Ar is entirely derived from the atmosphere. The lower ASW concentrations are those with no excess air component and the higher values are those with a 50 % excess air component

significant addition of ^4He to the groundwater samples. Measured ^4He concentrations in the injected water were an order of magnitude higher, with the calculated ^4He concentration of water in equilibrium with the produced fluid samples being over another order of magnitude higher still. As with ^4He the lowest ^{40}Ar concentration was that calculated for water in equilibrium with the injected CO_2 under reservoir conditions (Fig. 27). The next highest were those calculated for water in contact with the produced fluids from the Weyburn field with the injected water having an order of magnitude higher ^{40}Ar concentration. The highest concentrations were those observed in the groundwater wells which were within the calculated air saturated water range.

Both ^{20}Ne and ^{36}Ar concentrations exhibited extremely similar concentration groups to ^{40}Ar, with the lowest observed in the calculated water

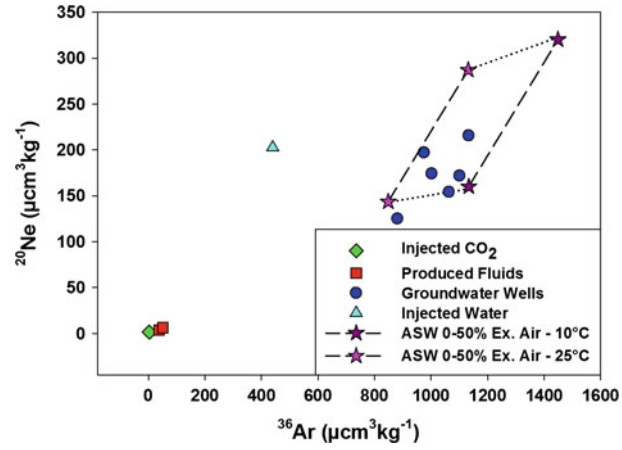

Fig. 28 ^{20}Ne concentrations plotted against ^{36}Ar concentrations. There is a pronounced difference in concentrations between the produced fluids and injected CO_2, the injected water and the groundwater samples. All but one of the groundwater samples can be explained by the calculated air saturated water concentration range, indicating that all of the ^{20}Ne and ^{36}Ar in the waters is atmosphere derived

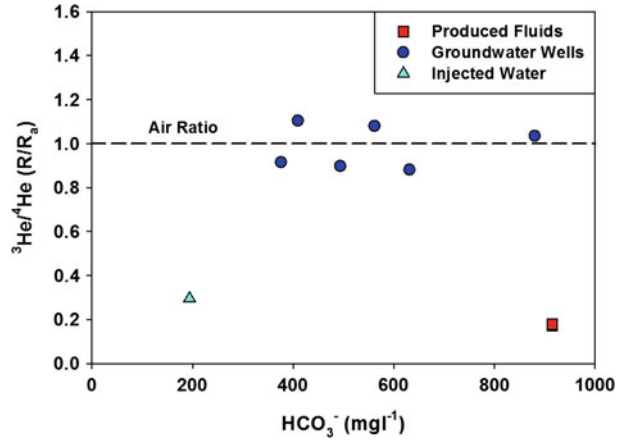

Fig. 29 ^{3}He/^{4}He ratios plotted against HCO_3^- concentrations in the produced reservoir fluids, groundwater wells and water injected into the reservoir surrounding the Kerr quarter. The *black dash line* indicates the air ^{3}He/^{4}He value of 1R$_a$. All of the groundwater wells have ^{3}He/^{4}He ratios which are close to the air ratio and exhibit no relationship between HCO_3^- concentrations and the ^{3}He/^{4}He ratio

concentration equilibrated with the injected CO_2 and highest being those observed in the groundwater wells (Fig. 28). As ^{20}Ne and ^{36}Ar are primarily derived from the atmosphere, this reinforced that the groundwater samples contained only atmospheric noble gases.

Gilfillan and Haszeldine (2011) observed no relationship between the ^{3}He/^{4}He ratio and HCO_3^- concentrations measured in the groundwaters from the Kerr site (Fig. 29). This is in stark contrast to the systematic relationship observed between HCO_3^- concentration and ^{3}He/^{4}He ratios in the St. Johns surface springs and groundwater wells (Sect. 7.3 and Fig. 23b). In the St. Johns Dome dataset there was a clear link between shallow samples and deep sources of CO_2 and He (Gilfillan et al. 2011). The majority of the St. Johns water samples

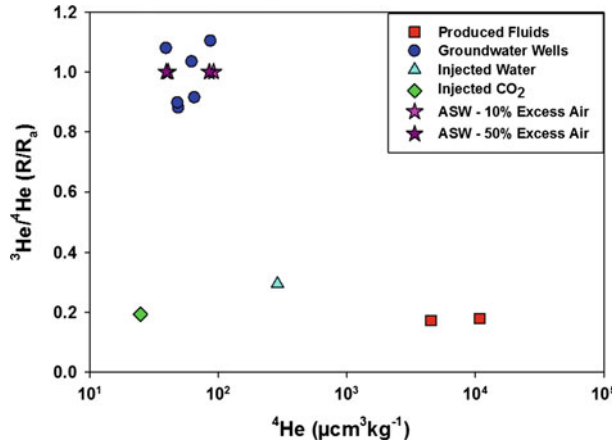

Fig. 30 $^{3}He/^{4}He$ plotted against ^{4}He concentrations in the produced reservoir fluids, groundwater wells and water injected into the reservoir surrounding the Kerr quarter. It is readily apparent that all of the groundwater samples exhibit ^{4}He concentrations which are within the air saturated water concentrations and there is no correlation to the either the injected water, injected CO_2 or produced fluids from the Weyburn oil field

exhibited higher HCO_3^- concentrations which corresponded to lower $^{3}He/^{4}He$ ratios and showed a clear trend towards the lower $^{3}He/^{4}He$ and higher HCO_3^- concentrations recorded in the deep CO_2 well water. In the Kerr groundwaters increased HCO_3^-, indicating increasing concentrations of dissolved CO_2 did not result in any variation in the air like $^{3}He/^{4}He$ ratios.

There was also no relationship observed between $^{3}He/^{4}He$ ratios and the concentration of ^{4}He in the Kerr groundwaters. This strongly implied that there is no addition of deep crustal ^{4}He to the sampled waters surrounding the Kerr quarter and indicates that there was no migration of fluids from depth into the sampled wells. This was again in contrast to the clear relationship between decreasing $^{3}He/^{4}He$ and increasing ^{4}He concentrations observed in the St. Johns groundwaters (Fig. 24a).

In summary, all of the noble gas concentrations and the majority of noble gas ratios measured in the groundwaters from wells surrounding the Kerr quarter were within or very close to the air saturated values. Gilfillan and Haszeldine (2011) found no evidence in any of the noble gas data that there was any presence of deep crustal derived noble gases within the groundwaters surrounding the Kerr quarter. Hence, they found no evidence of the migration of deep CO_2 from the Weyburn oil field into the groundwater on the Kerr quarter or the surrounding area (Fig. 30).

8 Summary and Future Work

Studies of noble gases in natural CO_2 storage analogues have proven to be extremely useful in establishing the viability of geological CO_2 storage. Noble gas data has shown that it is possible to store CO_2 for significant periods of time (up to 40 million years in the case of one reservoir). Measurements of noble gases and carbon stable isotopes have also permitted the identification of the main CO_2 storage processes that act in natural CO_2 reservoirs over geological timescales providing important lessons for engineered storage. These data indicate that the dominant mechanism of CO_2 loss is through dissolution of CO_2 into the formation water within a narrow pH window (pH = 5–5.8). Precipitation of carbonate minerals is only a minor sink, accounting for a maximum of 18 % of CO_2 loss in one of the CO_2 reservoirs.

For CO_2 storage technology to be universally deployed, it is essential that a robust, reliable and inexpensive means to trace the migration of CO_2 within the subsurface exists. Monitoring

during injection will increase confidence that the site characteristics were correctly determined and met. Furthermore, should migration and subsequent surface leakage occur, the ability to track origin and ownership of CO_2 at near and ground surface will be critical for remediation purposes. However, one of the key necessities of any monitoring program will be the detection of any migration, however small, of CO_2 from the storage site. The main problem in detecting migration is the large variation in CO_2 concentrations within the Earth's crust. This makes unequivocally determining if detected small quantities of CO_2 are the result of migration of CO_2 from a storage site extremely difficult. The use of tracers is the main technique that could be used to accurately determine if migration of CO_2 from a storage site has occurred.

Noble gases are chemically inert, persistent and environmentally safe—and possess significant potential as tracers of CO_2 migration within future storage sites. Their ability to trace CO_2 migration within a reservoir is illustrated by the study undertaken at the Mabee EOR field (Sect. 6.1). They have the potential to be extremely useful in tracing migration of CO_2 once it has migrated outside a reservoir as highlighted by the St. Johns Springs and Green River studies (Sects. 7.2 and 7.3), and also can play an important role in investigations of alleged leakage, as outlined by the Weyburn investigation (Sect. 7.4). Hence, there is enormous promise in the use of noble gases to monitor for any leakage of CO_2 or CO_2 rich groundwater from an engineered storage site and so provide a means of reassurance of the security of the storage site. This promise will only be fulfilled if more studies similar to those highlighted in this chapter are undertaken. It is imperative that the many upcoming pilot CO_2 injection studies continue to investigate the behaviour of noble gases in the subsurface and develop suitable noble gas monitoring strategies.

Whilst the aspirations for future CO_2 emissions reduction are in increasing energy efficiency and in developing alternative and renewable energy technologies, these cannot fulfil our current demands for energy. The amount of time that it will take to develop these technologies, and the fact that there are still plentiful supplies of fossil fuels in developing countries, means their combustion will remain the main source of global energy for a considerable time to come. Capturing and storing the CO_2 produced by fossil fuel combustion can drastically reduce CO_2 emissions and this technology can be operational very soon, given the right support. The lessons learned from noble gas studies show that CO_2 can be safely stored on geological timescales and that any migration from a storage site could be detected. CCS has the potential to act as a 'bridge technology' significantly reducing emissions whilst other low carbon energy technologies are developed and deployed. The fossil fuel power plants will be built anyway, as the world needs a reliable economic source of energy. Therefore, the only question to be answered is whether we are willing to build the bridge to capture and store CO_2 emissions from these plants, or prepare to face the climate change consequences.

References

Allis R, Bergfeld D, Moore J, McClure K, MorganC, Chidsey T, Heath JE, McPherson B (2005) Implications of results from CO_2 flux surveys over known CO_2 systems for long-term monitoring.In: Fourth annual conference on carbon capture and sequestration, DOE/NETL, 2–5 May 2005

Allis R, Chidsey T, GwynnW, Morgan C, White S, Adams M, Moore J (2001) Natural CO_2 reservoirs on the colorado plateau and southern rocky mountains: candidates for CO_2 sequestration. DOE/NETL: 1st National conference of carbon sequestration. Procedings Volume

Baines SJ, Worden RH (2004a) Geological storage of carbon dioxide. In: Baines SJ, Worden RH (eds) Geological storage of carbon dioxide. The Geological Society of London, London, pp 1–6

Baines SJ, Worden RH (2004b) The long term fate of CO_2 in the subsurface: natural analogues for CO_2 storage. In: Bains SJ, Worden RH (eds) Geological storage of carbon dioxide. Geological Society, London, pp 59–85

Ballentine CJ, O'Nions RK, Coleman CL (1996) A magnus opus: helium, neon and argon isotopes in a North Sea oilfield. Geochimica Cosmochim Acta 60:831–849

Ballentine CJ (1997) Resolving the mantle He/Ne and crustal 21-Ne/22-Ne in well gases. Earth Planet Sci Lett 152:233–249

Ballentine CJ, Schoell M, Coleman D, Cain BA (2001) 300-Myr-old magmatic CO_2 in natural gas reservoirs of the west Texas Permian basin. Nature 409:327–331

Ballentine CJ, Burgess R, MartyB (2002) Tracing fluid origin, transport and interaction in the crust. In: Porcelli DR, Ballentine CJ, Weiler R (eds) Noble gases in geochemistry and cosmochemistry, pp 539–614

Ballentine CJ, BurnardPG (2002) Production, release and transport of noble gases in the continental crust. In: Porcelli DR, BallentineCJ, Weiler R (eds) Noble gases in geochemistry and cosmochemistry, pp 481–538

Ballentine CJ, Marty B, Lollar BS, Cassidy M (2005) Neon isotopes constrain convection and volatile origin in the Earth's mantle. Nature 433:33–38

Battani A, Deville E, Faure JL, Jeandel E, Noirez S, Tocqué E, Benoît Y, Schmitz J, Parlouar D, Sarda P, Gal F, Le Pierres K, Brach M, Braibant G, Beny C, Pokryszka Z, Charmoille A, Bentivegna G, Pironon J, de Donato P, Garnier C, Cailteau C, Barrès O, Radilla G, Bauer A (2010) Geochemical study of natural CO_2 emissions in the French Massif Central: how to predict origin, processes and evolution of CO_2 leakage. Oil Gas Sci Technol: Rev IFP 65(4):615–633

Battani A, Sarda P, Prinzhofer A (2000) Basin scale natural gas source, migration and trapping traced by noble gases and major elements: the Pakistan Indus basin. Earth Planet Sci Lett 181(1–2):229–249

Becker J (2005) Quantification of Himalayan Metamorphic CO2 fluxes: impact on global carbon budgets. PhD thesis, University of Cambridge, Cambridge. UK

Bosch A, Mazor E (1988) Natural-gas association with water and oil as depicted by atmodspheric Noble Gases—Case studies from the southeastern mediterranean coastal-plain. Earth Planet Sci Lett 87(3): 338–346

Bradshaw J, Boreham C, La Pedalina F (2004) Storage retention time of CO_2 in sedimentary basins; examples from petroleum systems. In: Rubin E, Keith D, Brewer PG, Friederich G, Peltzer ET, Orr FM Jr (1999) Direct experiments on the Ocean disposal of fossil fuel CO_2. Science 284:943–945

Brewer PG, Friederich G, Peltzer ET, Orr FM Jr (1999) Direct experiments on the Ocean disposal of fossil fuel CO2. Science 284(5416):943–945. doi: 10.1126/science.284.5416.943

Broadhead RF (1998) Natural accumulations of carbon dioxide in the New Mexico region—Where are they, how do they occur and what are the uses for CO2? Lite Geol 20:2–6

Brohan P, Kennedy JJ, Harris I, Tett SFB, Jones PD (2006) Uncertainty estimates in regional and global observed temperature changes: a new data set from 1850. J Geophys Res 111(D12):D12106 doi: 10.1029/2005jd006548

Burnard P, Graham D, Turner G (1997) Vesicle-specific noble gas analyses of "Popping Rock": implications for primordial Noble Gases in Earth. Science 276:568–570

Burnard PG, Graham DW, Farley KA (2002) Mechanisms of magmatic gas loss along the Southeast Indian Ridge and the Amsterdam -St. Paul Plateau. Earth Planet Sci Lett 203:131

Casanova J, Bodénan F, Négrel P, Azaroual M (1999) Microbial control on the precipitation of modern ferrihydrite and carbonate deposits from the Cézallier hydrothermal springs (Massif Central, France). Sed Geol 126(1–4):125–145. doi:10.1016/s0037-0738(99)00036-6

Castro MC, Goblet P (2003) Calibration of regional groundwater flow models: working toward a better understanding of site-specific systems. Water Resouces Res 39:1172

Castro MC, Goblet P, Ledoux E, Violette S, de Marsily G (1998) Noble gases as natural tracers of water circulation in the Paris Basin 2. Calibration of a groundwater flow model using noble gas isotope data. Water Resouces Res 34:2467–2483

Cathles LM, Schoell M (2007) Modeling CO_2 generation, migration and titration in sedimentary basins. Geofluids 7:441–450

Craig H, Lupton JE, Horibe Y (1978) A mantle helium component in circum Pacific volcanic gases. In: Alexander EC, Ozima M (eds) Terrestrial rare gases. Japan Science Societies Press, Tokyo, pp 3–16

Deines P, Langmuir D, Harmon RS (1974) Stable carbon isotopes and the existence of a gas phase in the evolution of carbonate groundwaters. Geochim Cosmochim Acta 38:1147–1184

Drescher J, Kirsten T, Schafer K (1998) The rare gas inventory of the continental crust, recovered by the KTB continental deep drilling project. Earth Planet Sci Lett 119:271–281

EU (2009) Directive 2009/31/EC of the European Parliament and of the Council on the geological storage of carbon dioxide. Official J Eur Union L140:114–136

Fanale FP, Cannon WA (1971) Physical adsorption of rare gases on terrigenous sediments. Earth Planet Sci Lett 11:362–368

Farley KA, Craig H (1994) Atmospheric argon contamination of ocean island basalt olivine phenocrysts. Geochim Cosmochim Acta 58:2509–2517

Fitton JG, James D, Leeman WP (1991) Basic magmatism associated with late cenozoic extension in the Western United-States—Compositional variations in space and time. J Geophys Res Solid Earth Planet 96(B8):13693–13711

Fontes J-Ch, Andrews JN, Walgenwitz F (1991) Évaluation de la production naturelle in situ d'argon-36 via le chlore-36: implications géochimiques et géochronologiques. C. R. Acad. 856 Paris 313, Série II, pp 649–654

Gautheron C, Moreira M (2002) Helium signature of the subcontinental lithospheric mantle. Earth Planet Sci Lett 199(1–2):39

Gilfillan SMV, Ballentine CJ, Holland G, Sherwood Lollar B, Stevens S, Schoell M, Cassidy M (2008) The noble gas geochemistry of natural CO_2 gas reservoirs from the Colorado Plateau and Rocky Mountain provinces, USA. Geochim Cosmochim Acta 72:1174–1198

Gilfillan SMV, Lollar BS, Holland G, Blagburn D, Stevens S, Schoell M, Cassidy M, Ding Z, Zhou Z, Lacrampe-Couloume G, Ballentine CJ (2009) Solubility trapping in formation water as dominant CO_2 sink in natural gas fields. Nature 458:614–618

Gilfillan SMV, Wilkinson M, Haszeldine RS, Shipton ZK, Nelson ST, Poreda RJ (2011) He and Ne as tracers of natural CO_2 migration up a fault from a deep reservoir. Int J Greenhouse Gas Control 5(6):1507–1516. doi:10.1016/j.ijggc.2011.08.008

Gilfillan SMV, Haszeldine RS 2011 Report of noble gas, carbon stable isotope and HCO3- measurements from the Kerr Quarter and surrounding area, Goodwater, Saskatchewan. In: Sherk GW (ed) The Kerr investigation: final report, vol. IPAC-CO_2 Research Inc, Regina

Goldberg DS, Takahashi T, Slagle AL (2008) Carbon dioxide sequestration in deep-sea basalt. Proc Nat Acad Sci 105:9920–9925

Graham D (2002) Noble gas isotope geochemistry of Mid-Ocean Ridge and Ocean Island Basalt: characterization of mantle source reservoirs. In: Porcelli D, Ballentine CJ, Wieler R (eds) Noble gases in geochemistry and cosmochemistry 47:247–317

Haszeldine RS (2009) Carbon capture and storage: how green can black be? Science 325:1647–1652

Heath JE (2004) Hydrogeochemical characterization of CO_2 charged fault zones: the Little Grand Wash and Salt Wash fault zones, Emery and Grand counties, Utah. PhD thesis Utah State University, Logan

Hilton D, Fischer T, Marty B (2002) Noble gases and volitile recycling at subduction zones. In: Porcelli DR, Ballentine CJ, Weiler R (eds) Noble gases in geochemistry and cosmochemistry 47:319–370

Hiyagon H, Kennedy BM (1992) Noble gases in CH_4-rich gas fields, Alberta, Canada. Geochimica Cosmochimica Acta 56:1569–1589

Holland G, Ballentine CJ (2006) Seawater subduction controls the heavy noble gas composition of the mantle. Nature 441(7090):186–191

Holland G, Cassidy M, Ballentine CJ (2009) Meteorite Kr in Earth's mantle suggests a late accretionary source for the atmosphere. Science 326:1522–1525

House KZ, Schrag DP, Harvey CF, Lackner KS (2006) Permanent carbon dioxide storage in deep-sea sediments. Proc Nat Acad Sci 103:12291–12295

IEA (2009) Technology roadmap: carbon capture and storage, Paris, p. www.iea.org

IPCC (2005) IPCC special report on carbon dioxide capture and storage. Cambridge University Press, Cambridge

IPCC (2007) Climate change 2007: synthesis report. Contribution of working groups I, II and III to the fourth assessment: report of the intergovernmental panel on climate change. IPCC, Geneva, Switzerland

Javoy M, Pineau F, Delorme H (1986) Carbon and nitrogen isotopes in the mantle. Chem Geol 57:41–62

Jenden PD, Hilton DR, Kaplan IR, Craig H (1993) Abiogenic hydrocarbons in and mantle helium in oil and gas fields. In: Howell DG (ed) The future of energy gases, U.S. Geological Survey Professional Paper 1570. U.S. Geological Survey, pp 31–56

Kennedy BM, Hiyagon H, Reynolds JH (1990) Crustal neon—A striking uniformity. Earth Planet Sci Lett 98:277–286

Kennedy BM, Torgersen T, van Soest MC (2002) Multiple atmospheric noble gas components in hydrocarbon reservoirs: a study of the Northwest Shelf, Delaware Basin, SE New Mexico. Geochim Cosmochim Acta 66:2807–2822

Kharaka YK, Cole DR, Hovorka SD, Gunter WD, Knauss KG, Freifeld BM (2006) Gas-water-rock interactions in Frio Formation following CO_2 injection: implications for the storage of greenhouse gases in sedimentary basins. Geology 34:577–580

Kipfer R, Aeschbach-Gertig W, Peeters F, StuteM (2002) Noble gases in lakes and groundwaters, noble gases in geochemistry and cosmochemistry, pp 615–700

Klara SM, Srivastava RD, McIlvried HG (2003) Integrated collaborative technology, development program for CO_2 sequestration in geologic formations—United States Department of Energy R&D. Energy Convers Manage 44:2699–2712

Kurz MD, Jenkins WJ (1981) The distribution of helium in oceanic basalt glasses. Earth Planet Sci Lett 53(1):41–54. doi:10.1016/0012-821x(81)90024-8

Lafleur P (2010) Geochemical Soil Gas Survey—a site investigation of SW30-5-13-W2 M, Weyburn Field, Saskatchewan. Petro-Find Geochem Ltd, Saskatoon

Mackintosh SJ, Ballentine CJ (2012) Using 3He/4He isotope ratios to identify the source of deep reservoir contributions to shallow fluids and soil gas. Chem Geol 304–305:142–150. doi:10.1016/j.chemgeo.2012.02.006

Marland G, Boden TA, Andres RJ (2008) Global, regional, and national fossil fuel CO_2 emissions, trends: a compendium of data on global change. Carbon Dioxide Information Analysis Center, Oak Ridge National Laboratory, U.S. Department of Energy, Oak Ridge, Tenn., USA

Marland G, Schlamadinger B (1999) The Kyoto Protocol could make a difference for the optimal forest-based CO_2 mitigation strategy: some results from GORCAM. Environ Sci Policy 2:111–124

Marty B, Jambon A (1987) $C/^3He$ in volatile fluxes from the solid Earth: implications for carbon geodynamics. Earth Planet Sci Lett 83:16–26

Marty B, O'Nions RK, Oxburgh ER, Martel D, Lombardi S (1992) Helium isotopes in alpine regions. Tectonophysics 206:71–78

Marty B, Zimmermann L (1999) Volatiles (He, C, N, Ar) in mid-ocean ridge basalts: assesment of shallow-level fractionation and characterization of source composition. Geochim Cosmochim Acta 63(21):3619–3633. doi:10.1016/s0016-7037(99)00169-6

Maughan EK (1988) Geology and petroleum potential, Colorado Park Basin Province, North-Central Colorado. US Geological Survey Open-File Report 88-450 E

Mazor E (1972) Paleotemperatures ans other hydrological parameters deduced from noble gases dissolved in groundwater, Jordan Rift Valley, Israel. Geochimica Cosmochimica Acta 36:1321–1326

Moore J, Adams M, Allis R, Lutz S, Rauzi S (2005) Mineralogical and geochemical consequences of the long-term presence of CO_2 in natural reservoirs: an example from the Springerville-St. Johns Field, Arizona, and New Mexico, USA. Chem Geol 217:365

Moreira M, Kunz J, Allegre C (1998) Rare gas systematics in popping rock: isotopic and elemental compositions in the Upper Mantle. Science 279:1178–1181

Nimz GJ, Hudson GB (2005) The use of noble gas isotopes for monitoring leakage of geologically stored CO_2. In: Thomas DC, Benson SM (eds) Carbon dioxide capture for storage in deep geologic formations. Elsevier, Amsterdam, pp 1113–1128

O'Nions RK, Oxburgh ER (1988) Helium, volatile fluxes and the development of continental crust. Earth Planet Sci Lett 90(3):331–347

Oxburgh ER, O'Nions RK, Hill RI (1986) Helium isotopes in sedimentary basins. Nature 324:632–635

Ozima M, Podosek PA (2001) Noble gas geochemistry, 2nd edn. Cambridge University Press, Cambridge

Pashin JC, McIntyr MR (2003) Temperature-pressure conditions in coalbed methane reservoirs of the Black Warrior basin: implications for carbon sequestration and enhanced coalbed methane recovery. Int J Coal Geol 54:167–183

Petroleum Technology Research Centre 2011 Response to a soil gas study by Petro-Find Geochem Ltd

Pinti DL, Marty B (1995) Noble gases in crude oils from the Paris Basin, France—implications for the origin of fluids and constraints on oil-water-gas interactions. Geochimica Cosmochimica Acta 59:3389–3404

Pinti DL, Marty B (1998) Separation of noble gas mixtures from petroleum and their isotopic analysis by mass spectrometry. J Chromatogr A 824(1):109–117

Pinti DL, Wada N, Matsuda J (1999) Neon excesses in pumice: volcanological implications. J Volcanol Geoth Res 88:279–289

Podosek PA (1980) Sedimentary noble gases. Geochim Cosmochim Acta 44:1875–1884

Porcelli D, Woolum D, Cassen P (2001) Deep earth rare gases: initial inventories, capture from the solar nebula, and losses during Moon formation. Earth Planet Sci Lett 193:237–251

Porcelli D, Ballentine CJ (2002) Models for the distribution of terrestrial noble gases and evolution of the atmosphere. Reviews in Mineralogy and Geochemistry 47:411–480

Porcelli D, Ballentine CJ, Wieler R (2002) An overview of noble gas—Geochemistry and cosmochemistry, noble gases in geochemistry and cosmochemistry, pp 1–19

Rahmstorf S (2010) A new view on sea level rise. Nat Rep Clim Change 4:44–45

Raistrick M, Mayer B, Shevalier M, Perez RJ, Hutcheon I, Perkins EH, Gunter WD (2006) Using chemical and isotopic data to quantify inoic trapping of carbon dioxide in oil field brines. Environ Sci Technol 40:6744–6749

Rauzi SL (1999) Carbon dioxde in the St. Johns—Springerville Area, Apache County, Arizonia. Arizonia Geological Survey, Open-File Report 99-2

Sarda P, Battani A, Prinzhofer A (2000) The 20Ne/36Ar ratio as a tracer for ancient oil: the oil–water and gas-water double distillation model. In: Goldschimidt 2000 vol 5(2). Cambridge Publications, Cambridge, p 876

Sarda P, Staudacher T, Allègre CJ et al (1985) $^{40}Ar/^{36}Ar$ in MORB glasses: constraints on atmosphere and mantle evolution. Earth Planet Sci Lett 72:357–375

Sherwood Lollar B, Ballentine CJ (2009) Insights into deep carbon derived from noble gases. Nat Geosci 2:543–547

Sherwood Lollar B, Ballentine CJ, O'Nions RK (1997) The fate of mantle-derived carbon in a continental sedimentary basin: integration of C/He relationships and stable isotope signatures. Geochim Cosmochim Acta 61:2295–2308

Sherwood Lollar B, O'Nions RK, Ballentine CJ (1994) Helium and neon isotope systematics in carbon dioxide-rich and hydrocarbon-rich gas reservoirs. Geochim Cosmochim Acta 58:5279

Sherwood Lollar B, Slater GF, Ahad J, Sleep B, Spivack J, Brennan M, MacKenzie P (1999) Contrasting carbon isotope fractionation during biodegradation of trichloroethylene and toluene: Implications for intrinsic bioremediation. Org Geochem 30:813–820

Shipton ZK, Evans JP, Kirschner D, Kolesar PT, Williams AP, J H (2004) Analysis of leakage through 'low-peameability' faults from natural reservoirs in the Colorado Plateau, east-central Utah. In: Baines SJ, Worden RH (eds) Geological storage of carbon dioxide. Geological Society, London, pp 43–58

Spycher N, Pruess K (2005) CO2-H2O mixtures in the geological sequestration of CO2. II. Partitioning Chloride Brines at 12–100°C and up to 600 bar. 69(13):3309

Stevens SH, Fox C, White T, Melzer S (2006) Natural CO2 analogs for Carbon Sequestration. Final Report for USDOE

Tolstikhin IN, Lehmann BE, Loosli HH, Gautschi A (1996) Helium and argon isotopes in rocks, minerals, and related groundwaters: a case study in northern Switzerland. Geochim Cosmochim Acta 60: 1497–1514

Torgersen T, Clarke WB (1985) Helium accumulation in groundwater, (i): an evaluation of sources and the continental flux of crustal ^{4}He in the Great Artesian Basin, Australia. Geochim Cosmochim Acta 49:1211–1218

Torgersen T, Kennedy B, van Soest M (2004) Diffusive separation of noble gases and noble gas abundance patterns in sedimentary rocks. Earth Planet Sci Lett 226:477–489

Torgersen T, Kennedy BM (1999) Air-Xe enrichments in Elk Hills oil field gases: role of water in migration and storage. Earth Planet Sci Lett 167:239–253

Treiloff M, Kunz J, Clague DA, Harrison D, Allegre CJ (2000) The nature of pristine noble gases in mantle plumes. Science 288:1036–1038

Trull T, Nadeau S, Pineau F, Polve M, Javoy M (1993) C-He systematics in hotspot xenoliths: Implications for mantle carbon contents and carbon recycling. Earth Planet Sci Lett 118:43

Wilkinson M, Gilfillan SMV, HaszeldineRS, BallentineCJ (2010) Plumbing the depths: testing natural tracers of subsurface CO_2 origin and migration, Utah. In: Grobe M, PashinJC, DodgeRL (eds) Carbon dioxide sequestration in geological media—State of the science. AAPG Studies

Woodward LA (1983) Geology and hydrocarbon potential of the raton basin, New Mexico. In: Fassett JE (ed) Oil and gas fields of the four corners area, vol 3. Four Corners Geological Society, pp 789–799

Wycherley H, Fleet A, Shaw H (1999) Some observations on the origins of large volumes of carbon dioxide accumulations in sedimentary basins. Mar Pet Geol 16:489–494

Zartman RE, Wasserburg GJ, Reynolds JH (1961) Helium, argon and carbon in some natural gases. J Geophys Res 66:277–306

Zhou Z, Ballentine CJ, Kipfer R, Schoell M, Thibodeaux S (2005) Noble gas tracing of groundwater/coalbed methane interaction in the San Juan Basin, USA. Geochim Cosmochim Acta 69:5413–5428